

惑星大気のスーパーローテーション

今村剛（東京大学）



Understanding the Diversity of Planetary Atmospheres

ISSN: 0038-6308 (Print) 1572-9672 (Online)

In this topical collection (9 articles)

ReviewPaper

A Review of Possible Planetary Atmospheres in the TRAPPIST-1 System

Martin Turbet, Emeline Bolmont, Vincent Bourrier...

» Download PDF (5077KB) » View Article

Article:100

ReviewPaper

Possible Atmospheric Diversity of Low Mass Exoplanets – Some Central Aspects

John Lee Grenfell, Jeremy Leconte, François Forget, Mareike Godolt...

Article:98

ReviewPaper

Future Missions to the Giant Planets that Can Advance Atmospheric Science Objectives

Mark D. Hofstadter, Leigh N. Fletcher, Amy A. Simon, Adam Masters...

Article:91

ReviewPaper

Is the Faint Young Sun Problem for Earth Solved?

Benjamin Charnay, Eric T. Wolf, Bernard Marty, François Forget

» Browse Volumes & Issues

Search within this journal

ReviewPaper

Superrotation in Planetary Atmospheres

Takeshi Imamura, Jonathan Mitchell, Sébastien Lebonnois...

» Download PDF (7002KB) » View Article

Article:87

ReviewPaper

Setting the Stage: Planet Formation and Volatile Delivery

Julia Venturini, María Paula Ronco, Octavio Miguel Guilera

Article:86

ReviewPaper

Comparison of the Deep Atmospheric Dynamics of Jupiter and Saturn in Light of the Juno and Cassini Gravity Measurements

Yohai Kaspi, Eli Galanti, Adam P. Showman, David J. Stevenson...

Article:84

ReviewPaper

Outstanding Challenges of Exoplanet Atmospheric Retrievals

Joanna K. Barstow, Kevin Heng

Article:82

ReviewPaper

How Well Do We Understand the Belt/Zone Circulation of Giant Planet Atmospheres?

Leigh N. Fletcher, Yohai Kaspi, Tristan Guillot, Adam P. Showman

» Download PDF (2376KB) » View Article

Article:30

Understanding the Diversity of Planetary Atmospheres

Europlanet & International Space Science Institute Workshop : 12-16 November 2018

Search



Workshop Objective Circulars Workshop Program Participants and Conveners Local Information

SSSI Book and Space Science Reviews Poster Restricted Area

SSSI Book and Space Science Reviews

Following the Workshop, its output will be published as a volume in the Space Science Series of ISSI by Springer (see <http://www.issibern.ch/publications>), in parallel with the publication of the papers in a Topical Collection in Space Science Reviews. It is expected that a total of up to 15 high-quality topical review papers will result. to be submitted to the

T. Imamura, J. Mitchell, S. Lebonnois, Y. Kaspi, A.P. Showman, O. Korablev,
Superrotation in planetary atmospheres. Space Sci. Rev. 216:87 (2020)

1 Introduction

- 1.1 Superrotation on Various Celestial Bodies *Imamura*
- 1.2 Dynamical Structure and Eddy Momentum Transport *Imamura*
- 1.3 Circulation Regimes *Mitchell*

2 Superrotation on Venus and Titan *Lebonnois*

- 2.1 Venus
- 2.2 Titan
- 2.3 What do We Learn when Comparing Venus and Titan?

3 Superrotation on the Gas Giants *Kaspi*

- 3.1 Observations of Jupiter and Saturn's Atmospheric Circulation
- 3.2 A Short History of Modeling Jupiter and Saturn's Zonal Flows
- 3.3 What do We Learn when Comparing Jupiter and Saturn?

4 Superrotation on Exoplanets *Showman*

- 4.1 Hot Jupiters
- 4.2 Tidally-Locked Terrestrial Exoplanets

5 Key Observations *Imamura, Korablev*

6 Concluding Remarks *Imamura*

Observed superrotating atmospheres

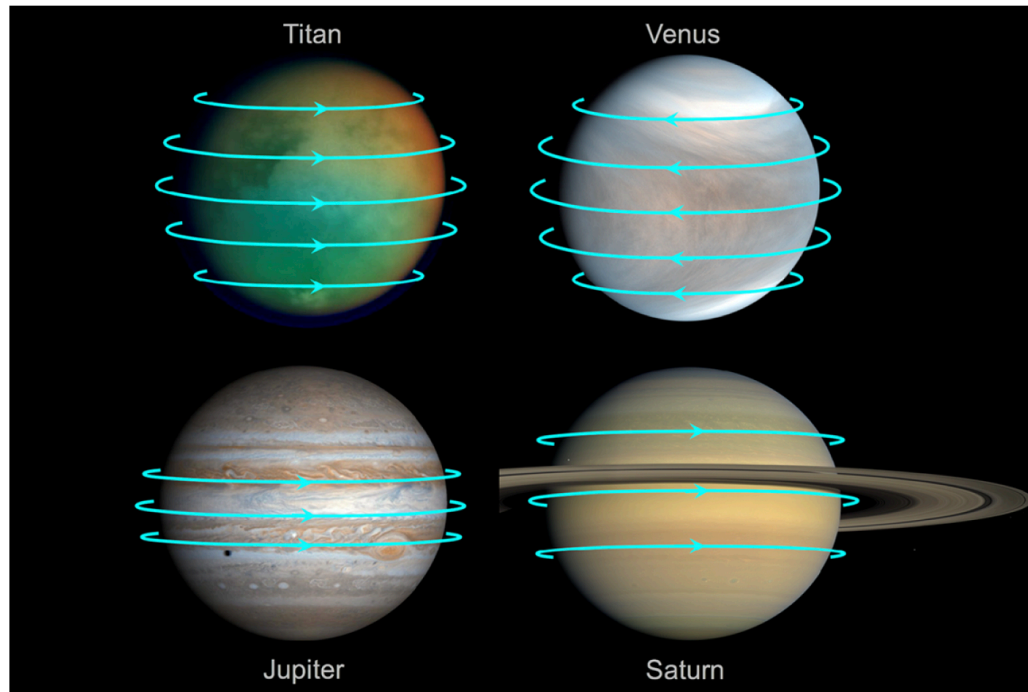
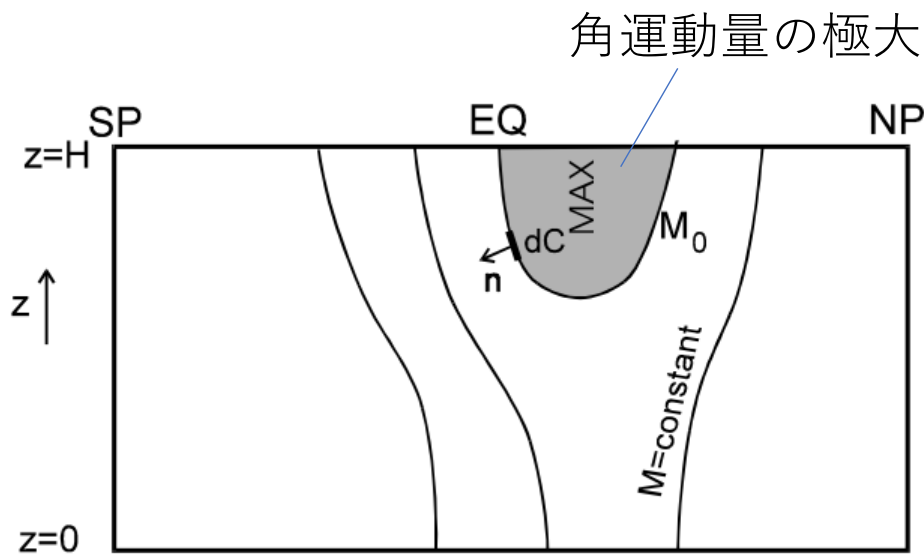


Table 1 Basic information on the superrotation of the atmospheres of the solar system planets and a hot Jupiter (modified from Read and Lebonnois 2018)

Planet	Radius (km)	Rotation period (days)	Equatorial rotation speed (m/s)	Equatorial wind speed (m/s)	Superrotation index, s , on the equator
Venus	6,052	243	1.81	100–120	55–66
Titan	2,576	16.0	11.7	100–180	8.5–15
Jupiter	69,911	0.41	12,300	60–140	0.005–0.011
Saturn	58,232	0.44	9,540	350–430	0.037–0.045
HD 189733b	79,500	2.2	2600	2400	0.92

Hide's theorem (1969)

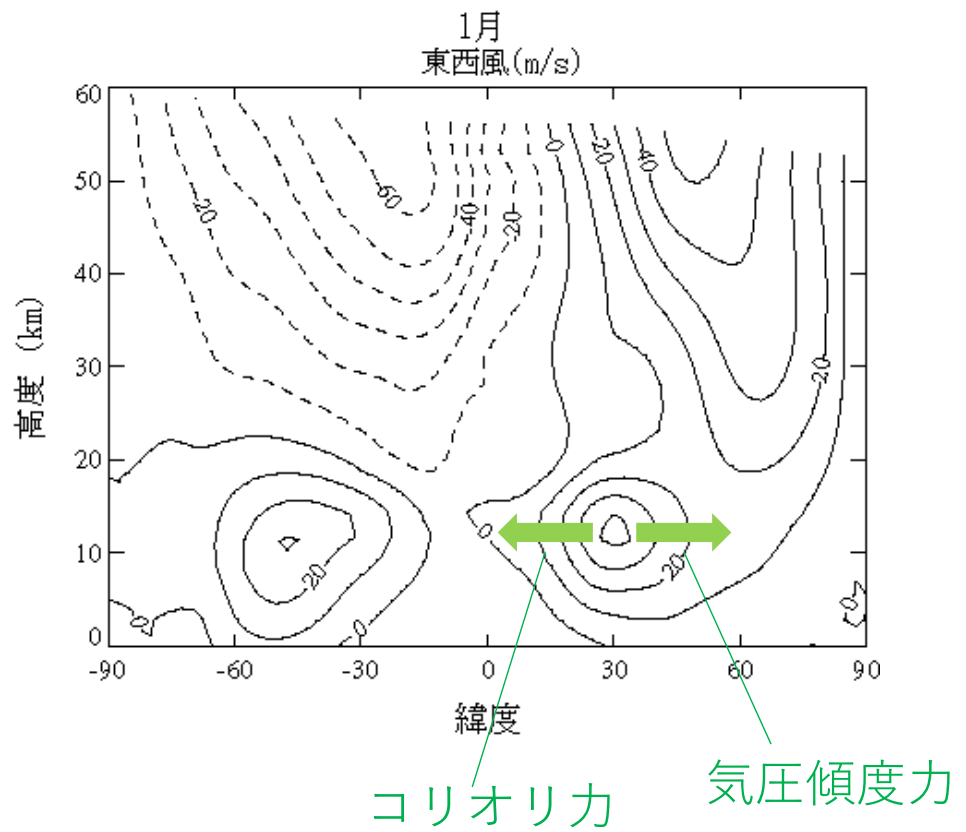
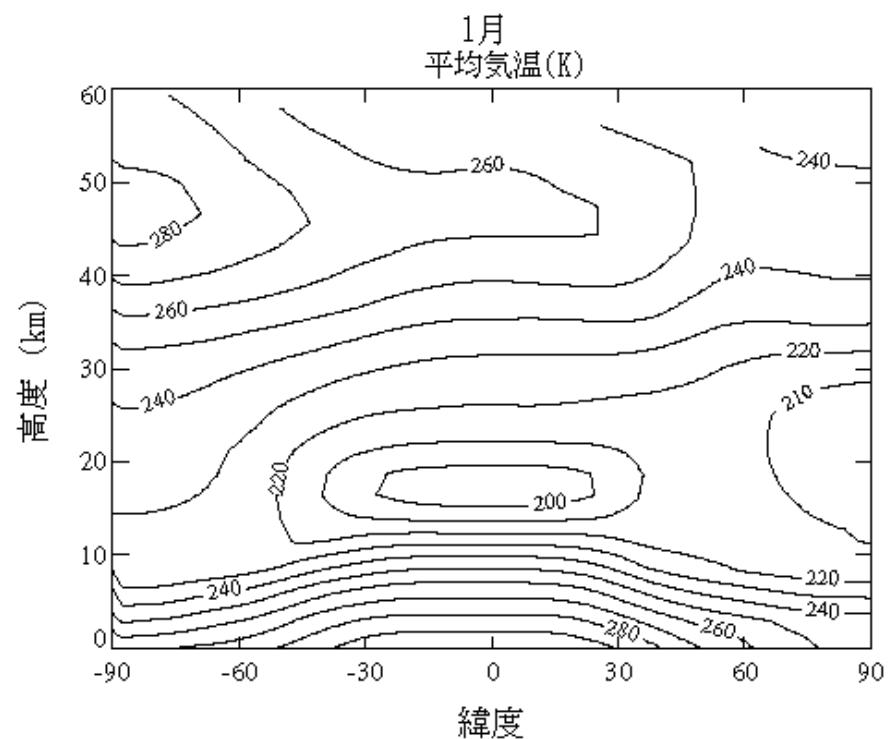
Non-axisymmetric eddies (waves) are needed to maintain the jets aloft the surface and that the required momentum convergence should be provided by upgradient angular momentum transport.



Vallis (2005)

Superrotation on Venus and Titan

地球における気温・東西風の子午面分布

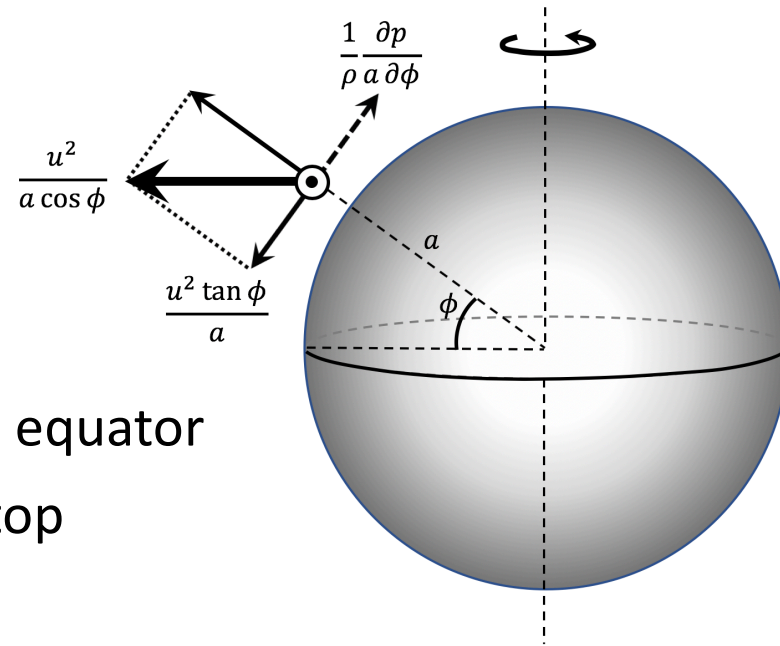


Cyclostrophic balance

In Venus's atmosphere

planetary rotation: 1.8 m/s on the equator

zonal wind: 100 m/s at the cloud top



Momentum equations

$$\frac{du}{dt} = \left(2\Omega \sin \phi + \frac{ut \tan \phi}{a} \right) v - \frac{uw}{a} - 2\Omega w \cos \phi - \frac{1}{\rho} \frac{\partial p}{\partial x}$$

$$\frac{dv}{dt} = - \left(2\Omega \sin \phi + \frac{ut \tan \phi}{a} \right) u - \frac{vw}{a} - \frac{1}{\rho} \frac{\partial p}{\partial y}$$

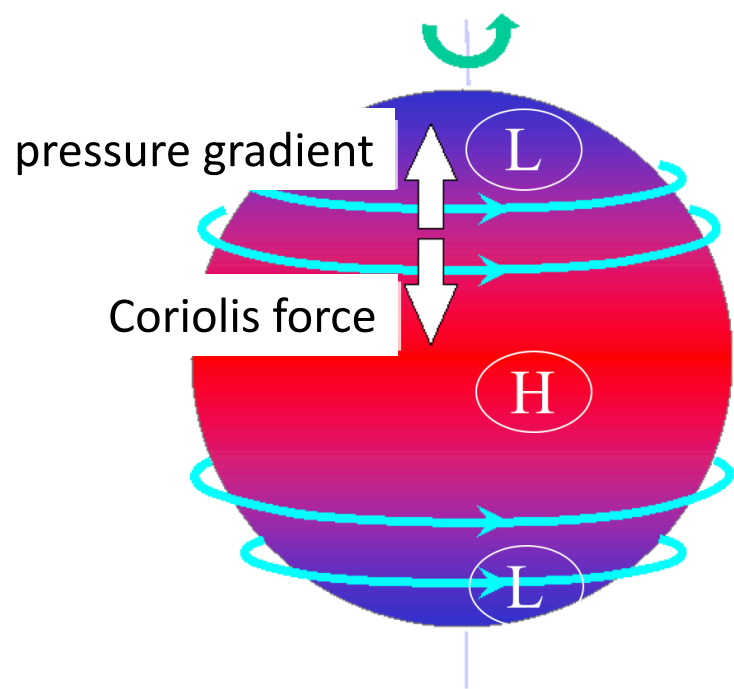
$$\frac{dw}{dt} = \frac{u^2 + v^2}{a} - 2\Omega u \cos \phi - \frac{1}{\rho} \frac{\partial p}{\partial z} - g$$

Atmospheric rotation takes the place of planetary rotation.

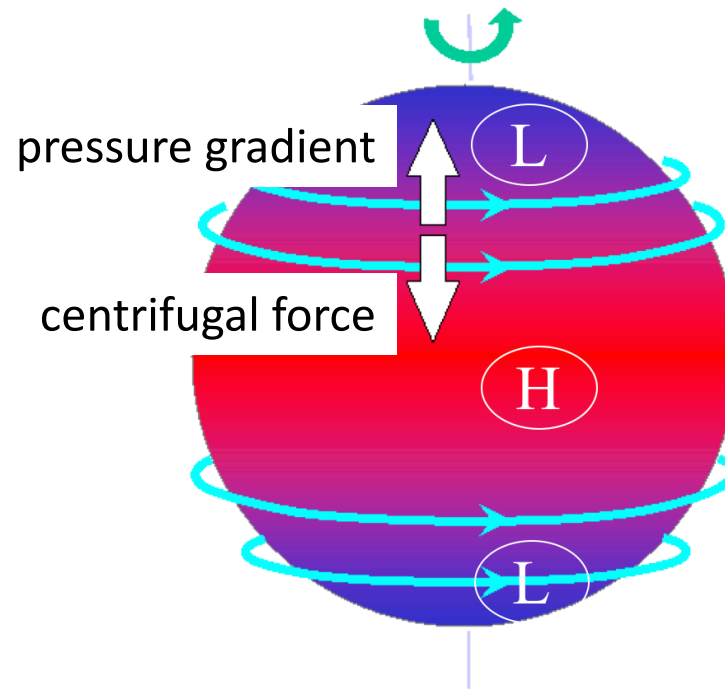
Meridional force balance of zonal flow

geostrophic flow
(planetary rotation \gg wind)

cyclostrophic flow
(planetary rotation \ll wind)

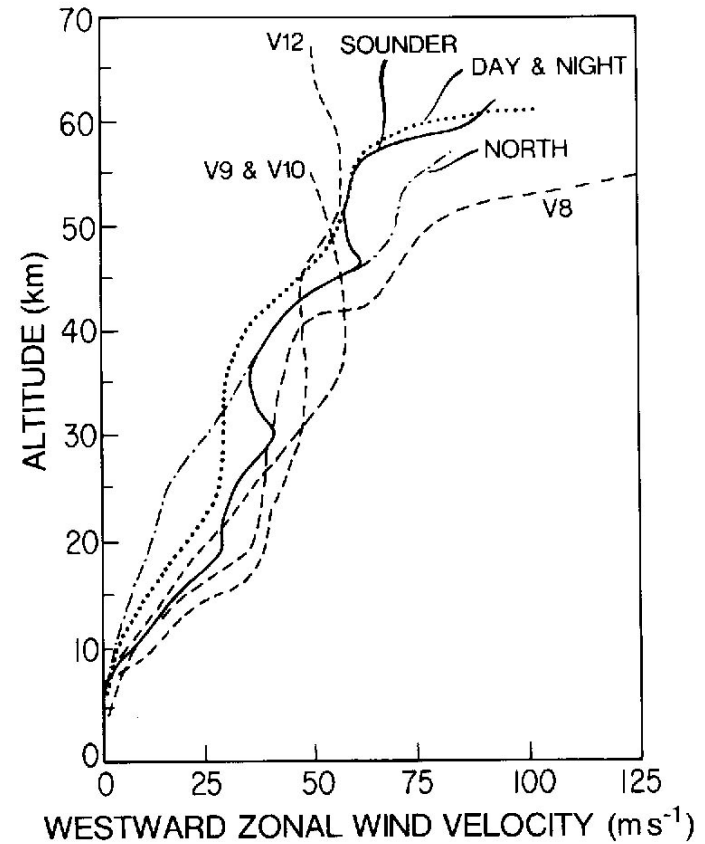


Earth-like



Venus-like

Superrotation of Venus' atmosphere



金星着陸機が測った風速の高度分布

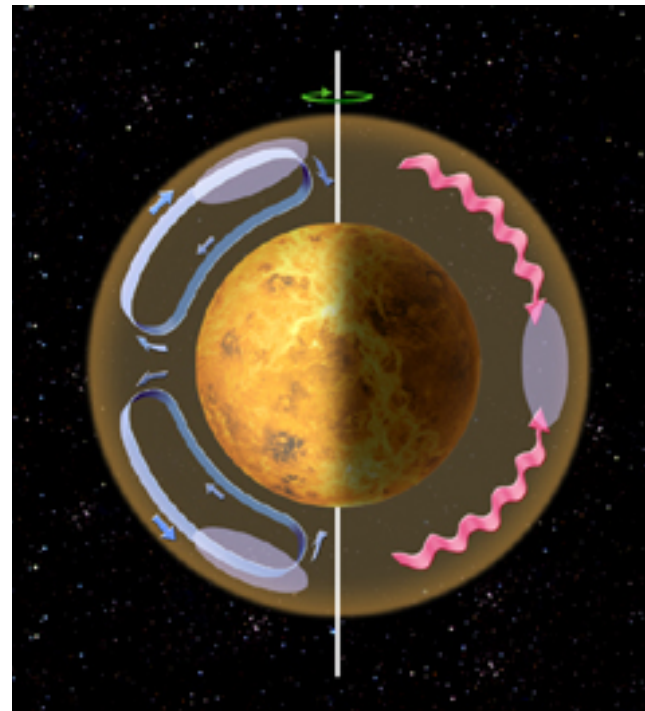
雲頂（65km）では大気が自転（周期243日）の60倍の速さで循環

子午面循環によるメカニズム

Gierasch-Rossow-Williams mechanism
(Gierasch, 1974; Rossow & Williams, 1979)

ハドレー循環

低緯度で角運動量を上向き輸送、高緯度で下向き輸送
高緯度ジェット生成



大規模水平擾乱

差動回転を解消
角運動量を赤道向きに輸送

大気上層に角運動量が蓄積

2D simulation in a slowly-rotating system

(Rossow & Williams 1979)

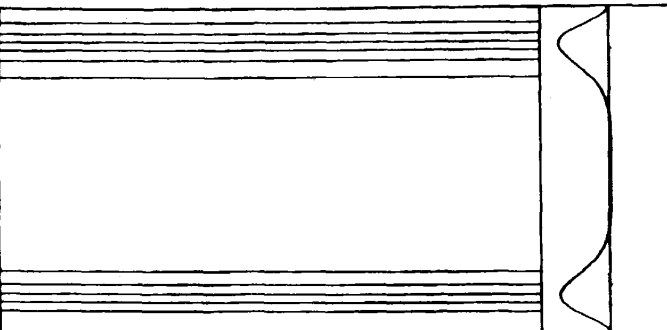
金星と同じ自転速度

高緯度でジェット型の強制

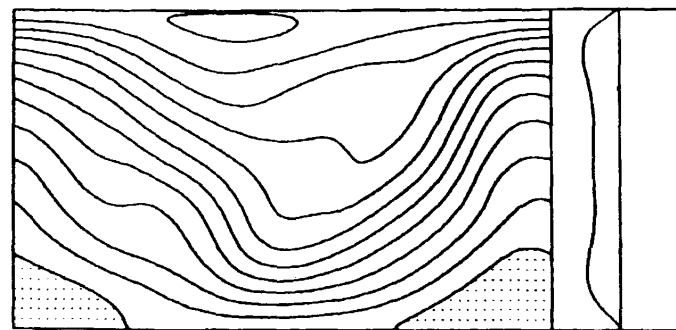
→順圧不安定(水平シアーよによる不安定)で擾乱生成、赤道向き角運動量輸送

観測的証拠はなし

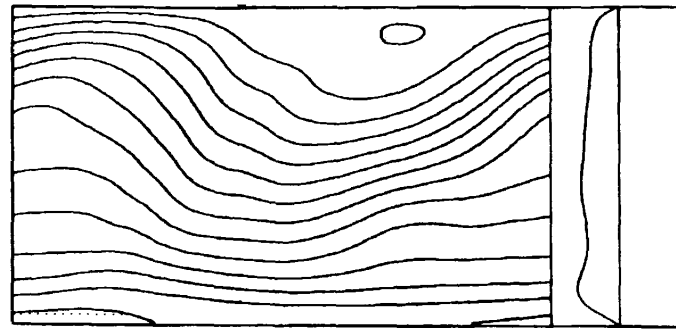
stream function



(a)



(b)



(c)

mean zonal
velocity

2.8 days

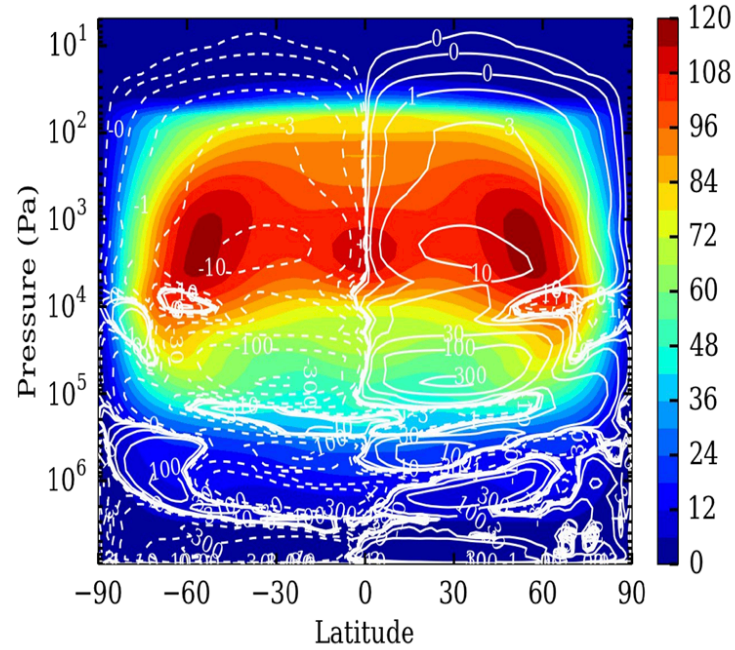
11.5 days

17.2 days

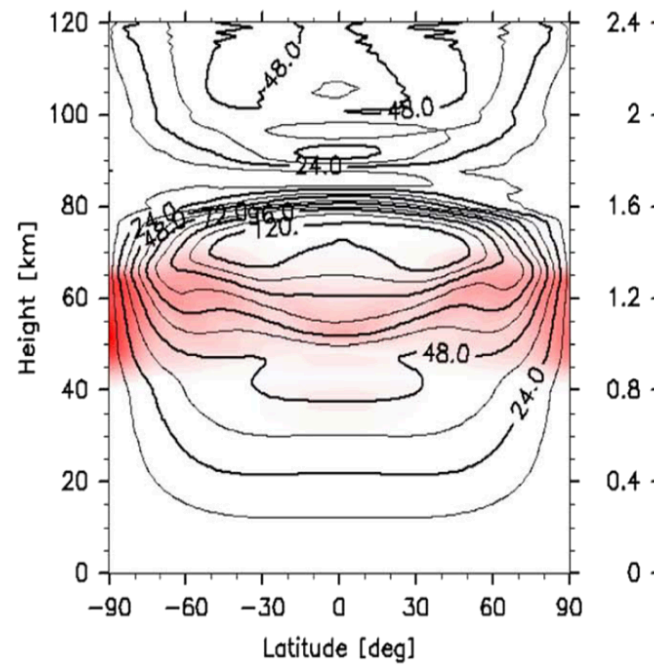
Numerical models

Zonal winds

Garate-Lopez and Lebonnois (2018)



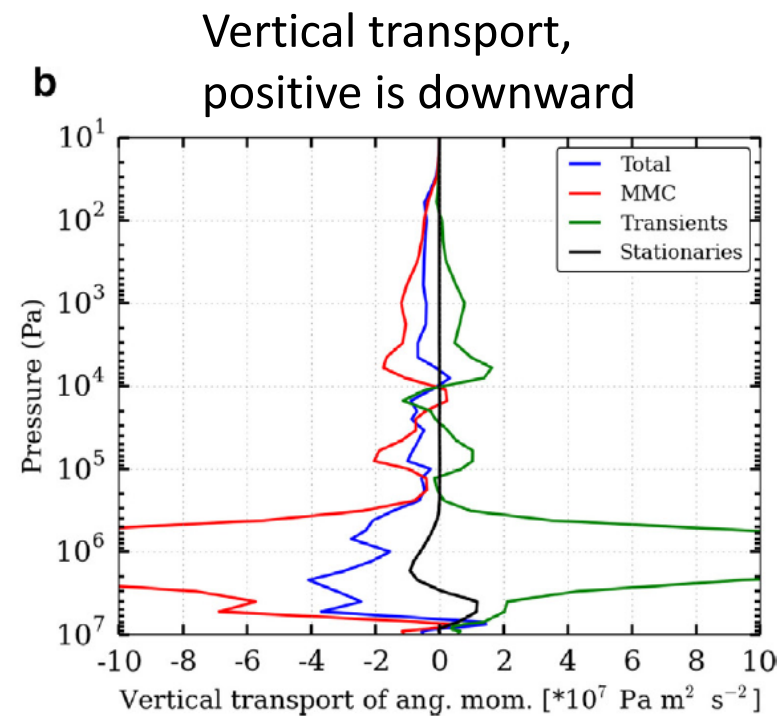
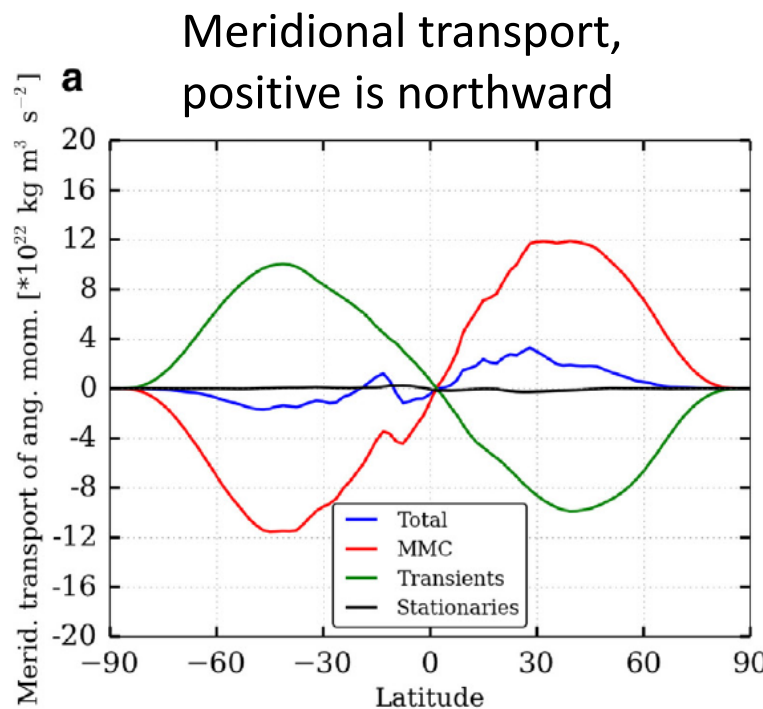
Sugimoto et al. (2014)



Numerical models

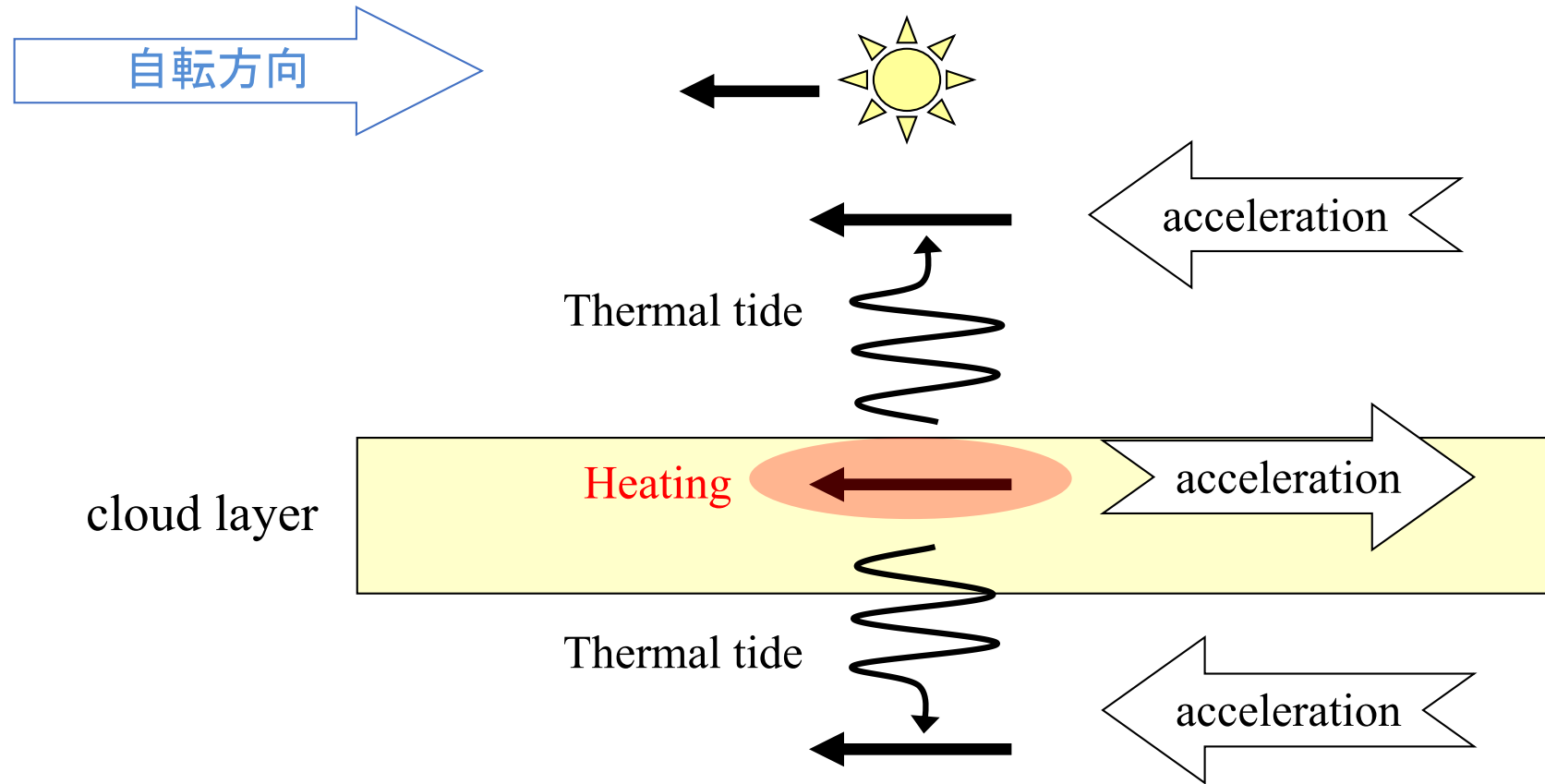
Transport of angular momentum

Lebonnois et al. (2016)



熱潮汐波によるメカニズム

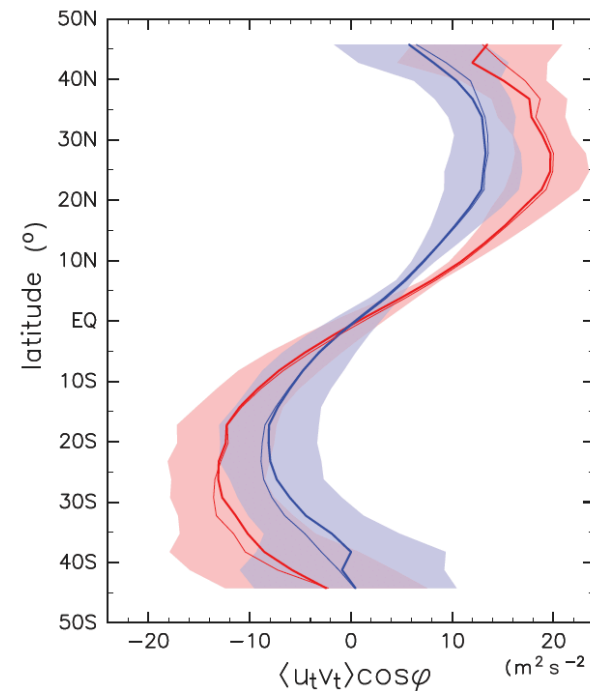
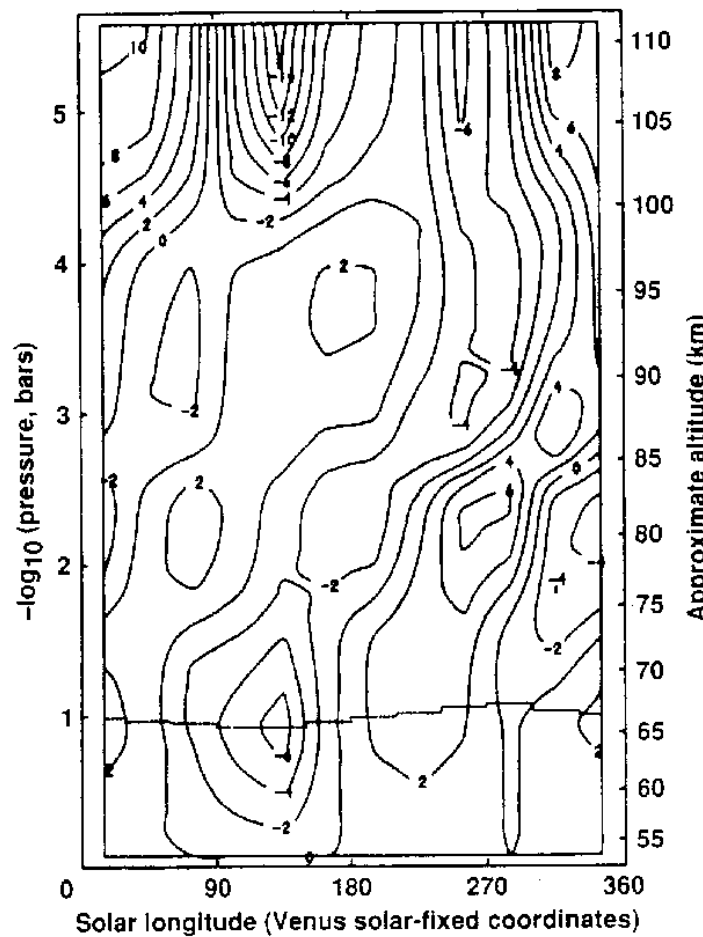
(Fels & Lindzen 1974; Takagi & Matsuda, 2006, 2008, ...)



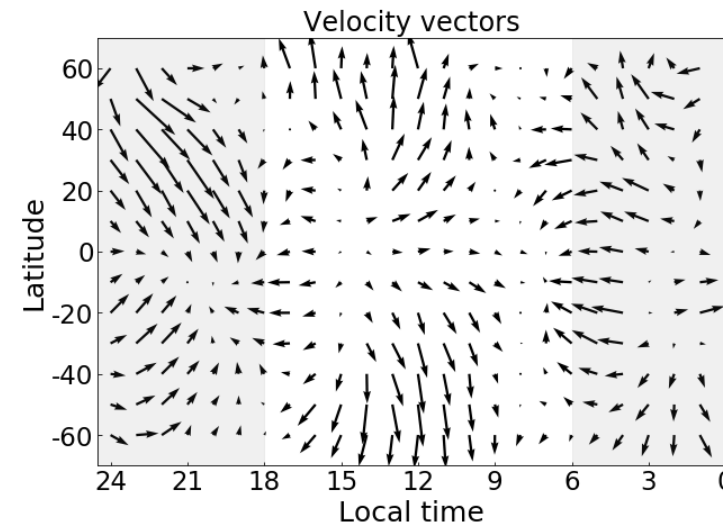
太陽光加熱域の移動により、東向き運動量を持つ重力波が励起されて
上下(+高緯度方向?)に伝搬 → 雲層が反動で西向きに加速

あかつきUVの雲追跡風から求めた角運動量の南北輸送
(Horinouchi et al. 2020)

Pioneer Venus赤外分光による成層圏
温度のローカルタイム-高度断面
(Schofield & Taylor 1983)

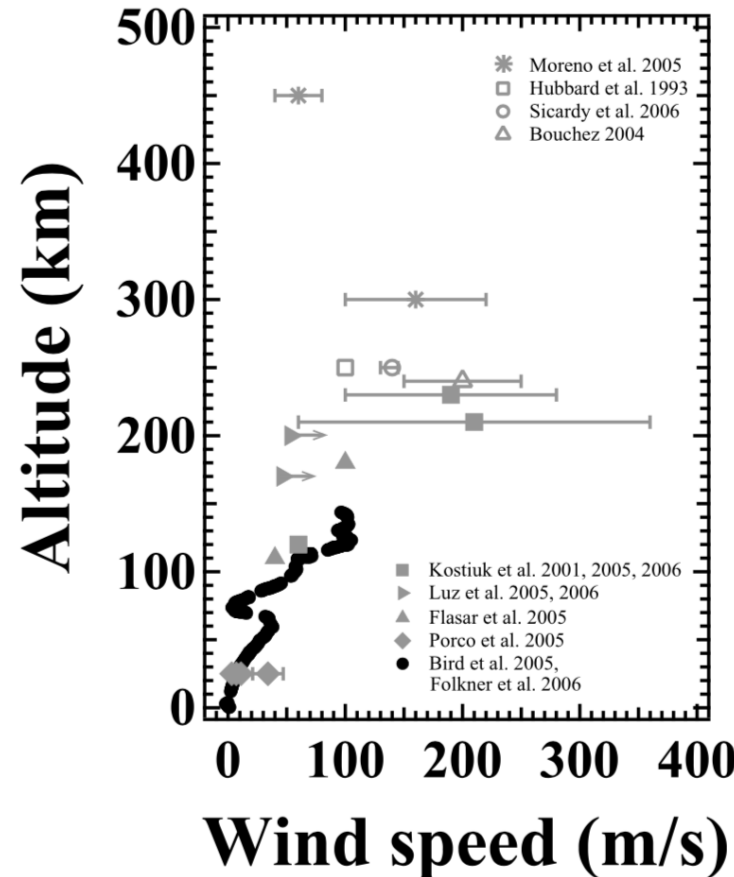
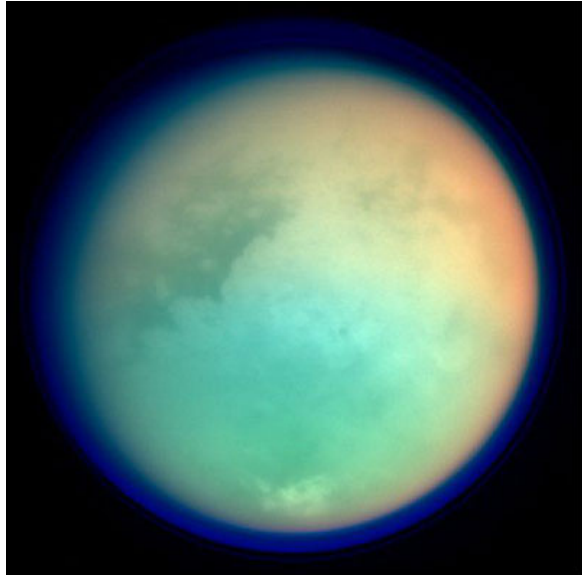


あかつき熱赤外の雲追跡風から求めたローカル
タイム固定風速場 (Fukuya, 投稿準備中)



Superrotation of Titan' atmosphere

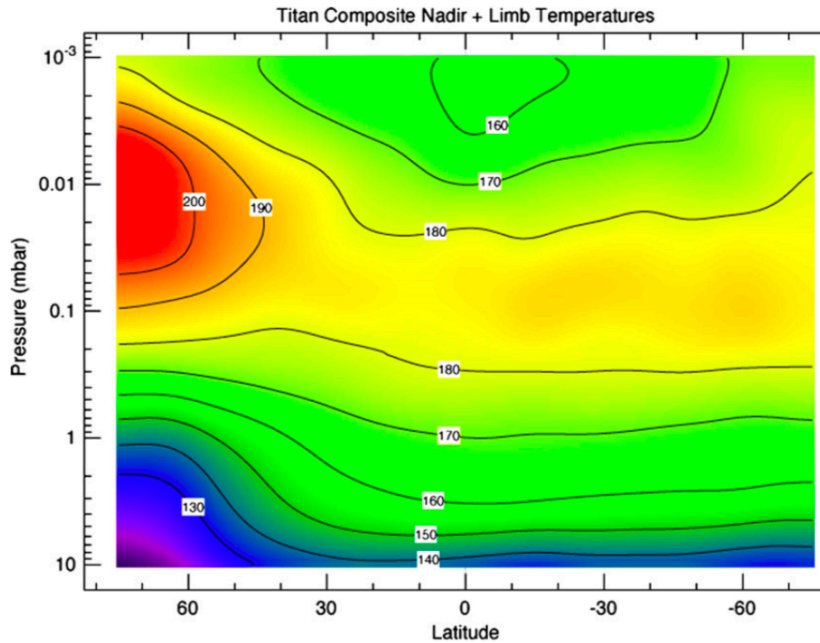
Hörst et al. 2017



上空では大気が自転(周期16日)の10倍の速さで
自転方向に循環

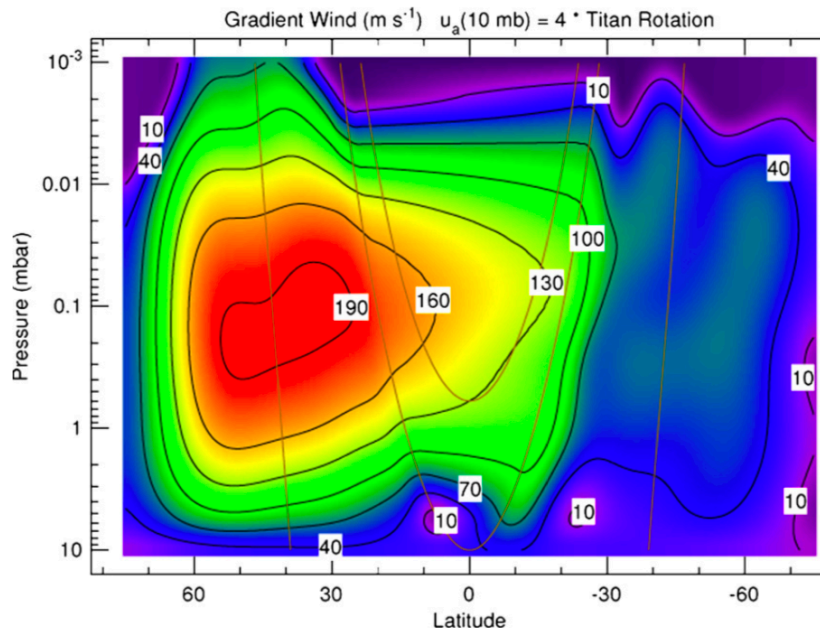
Infrared observation by CIRS on NASA Cassini (northern winter)

Achterberg et al. 2008



Zonal-mean
temperature

Fig. 9. Zonal mean temperatures from all limb and nadir maps. Retrieved temperatures were averaged in 5° latitude bins, then smoothed with a 10° boxcar function applied three times. Contours are labeled in K.



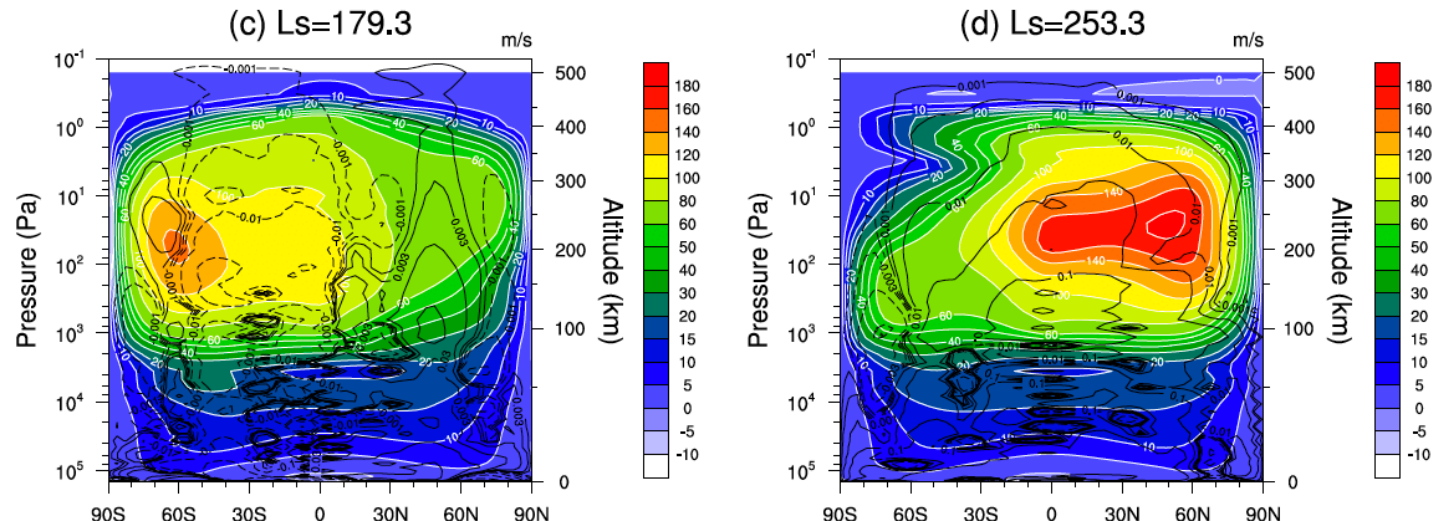
Zonal winds calculated
from the temperature
using thermal wind
relation

Fig. 10. Zonal winds calculated from the temperatures in Fig. 9 from the gradient wind equation, assuming solid-body rotation at the 10 mbar level at four times Titan's rotation rate. Wind speed contours (black lines) are labeled in m s^{-1} . The gray lines indicate cylindrical surfaces parallel to the rotation axis along which the gradient wind equation is integrated. Equatorward and above the gray line tangent to the equator at 10 mbar, the winds are unconstrained by the gradient wind equation, and have been linearly interpolated on constant pressure surfaces.

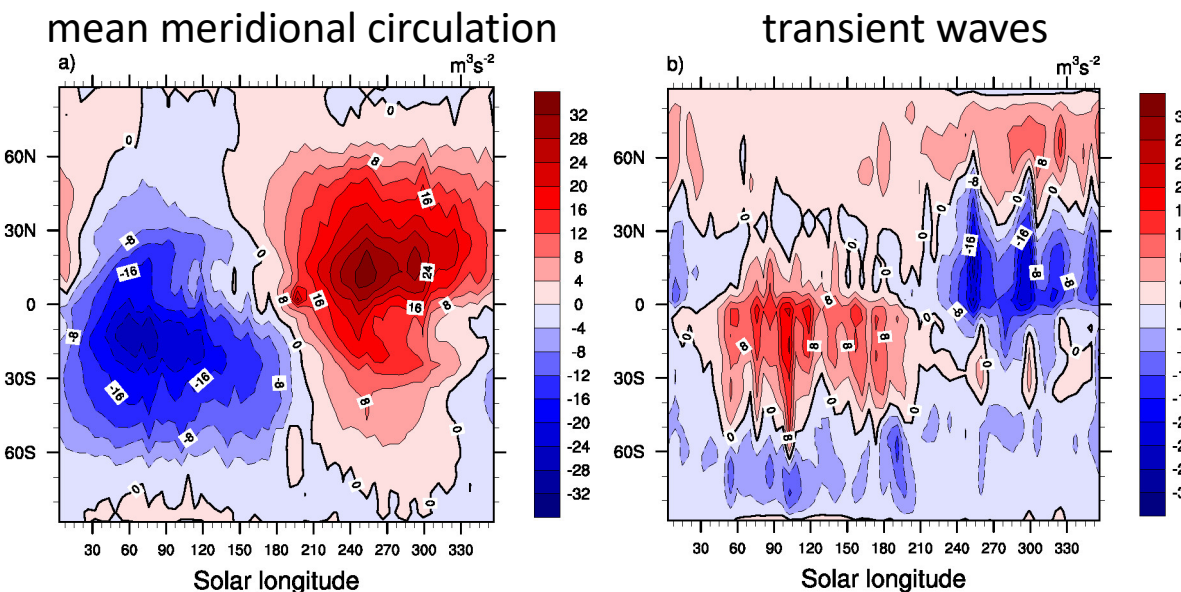
Numerical models

Lebonnois et al. (2012)

Mean zonal wind and meridional stream function



Seasonal variations of the vertically-integrated latitudinal transport of angular momentum



金星-タイタン比較

- タイタンのように季節変化が顕著でも年平均では金星と似たような子午面循環と角運動量バランスになる
- 熱潮汐は金星では効果的だがタイタンでは重要でない
- 金星とタイタンの共通点として、日射の大半が大気中で吸収されて地面にはほとんど届かないこと、熱慣性が大きく放射時定数が長いこと、が挙げられる（金星では30年、タイタンでは100年）

Circulation regimes

Parameter study of the atmospheric circulation of Earth-like planets with general circulation models (GCMs)

Williams (1988)

Zonal velocity

white : eastward

shade : westward

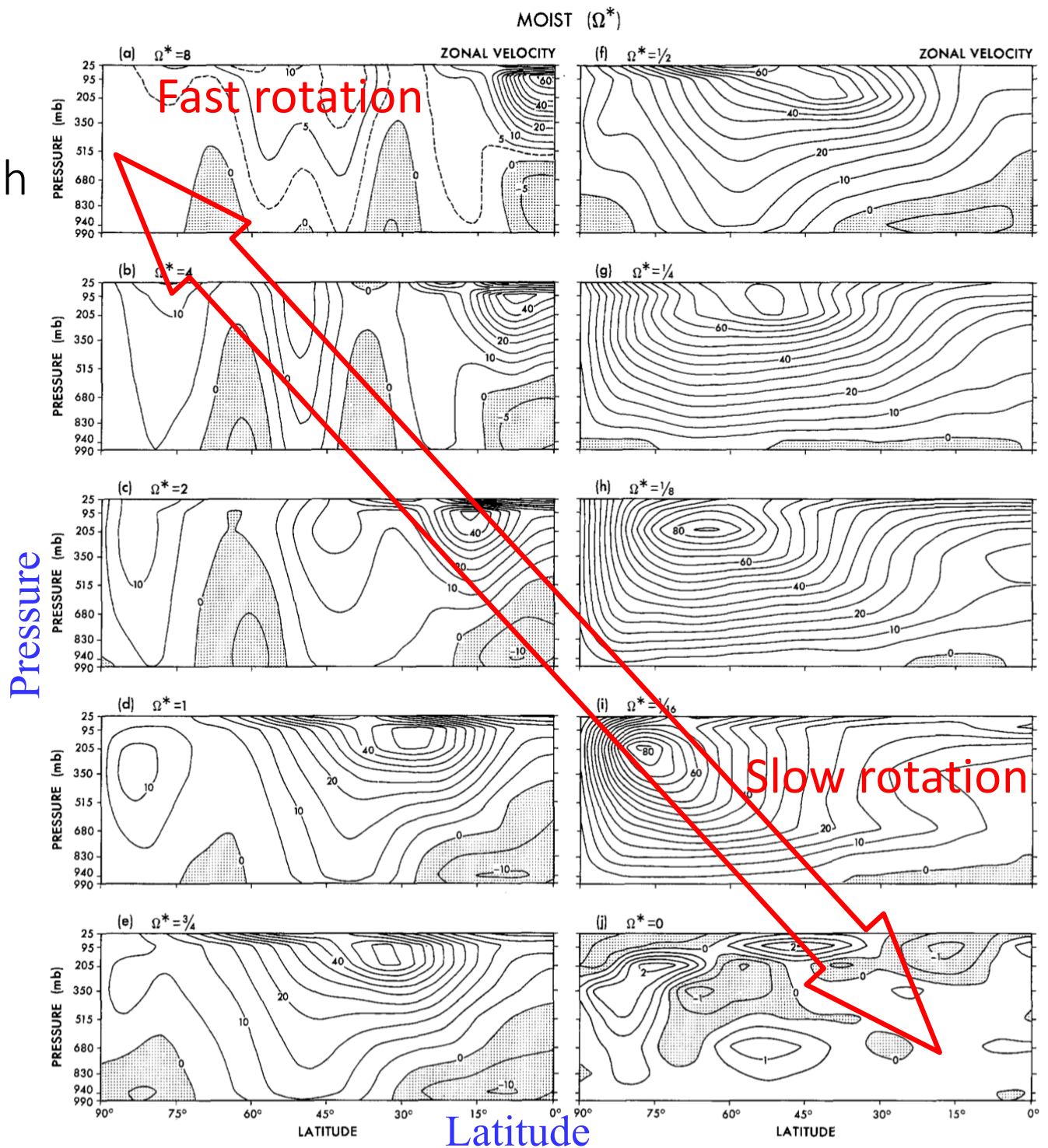


Fig. 2. Meridional distribution of the mean zonal wind for the MOIST model with $\Omega^* = 0-8$. Units: m s^{-1}

Meridional stream function

white : anti-clockwise

shade : clockwise

Williams (1988)

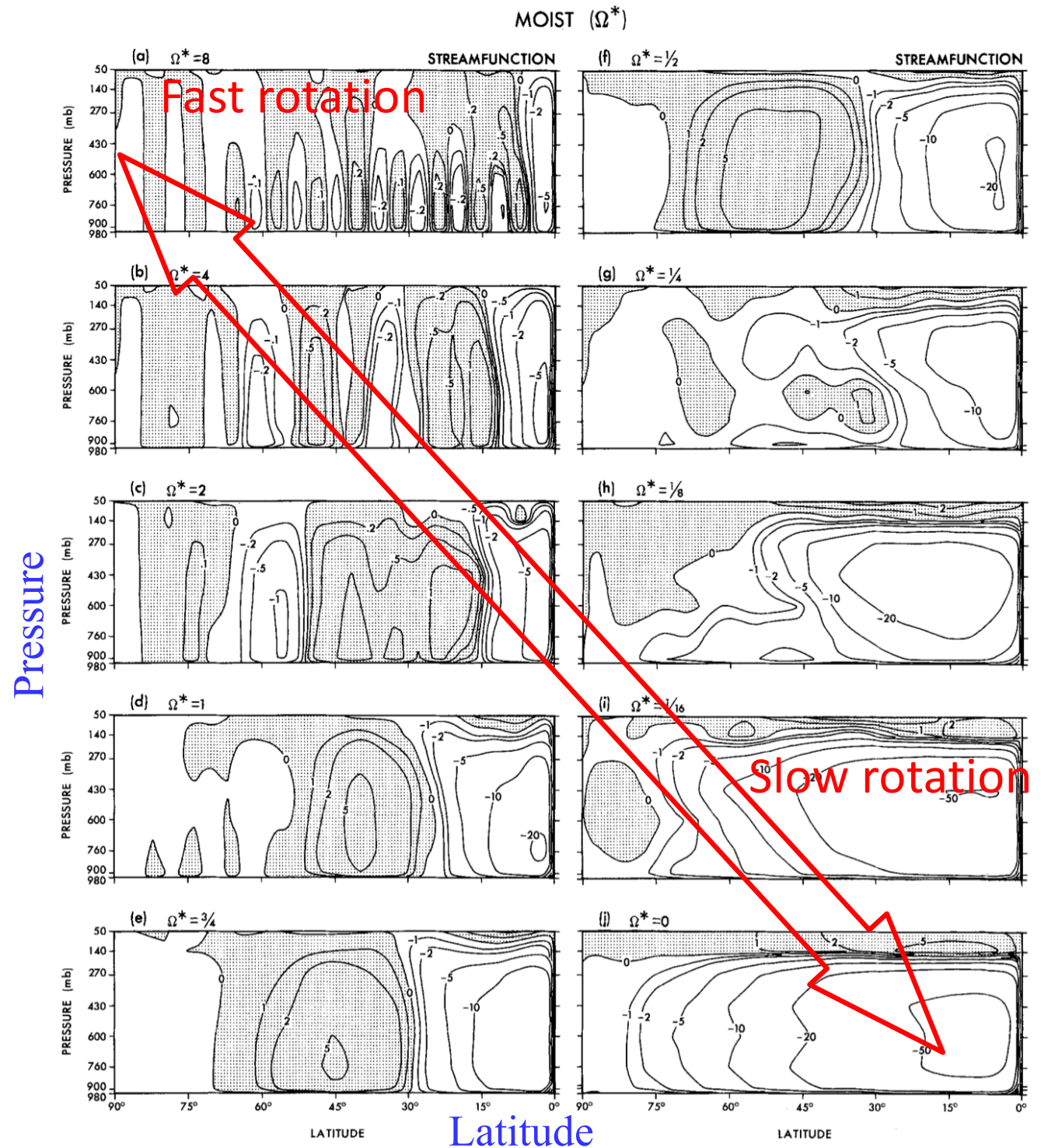
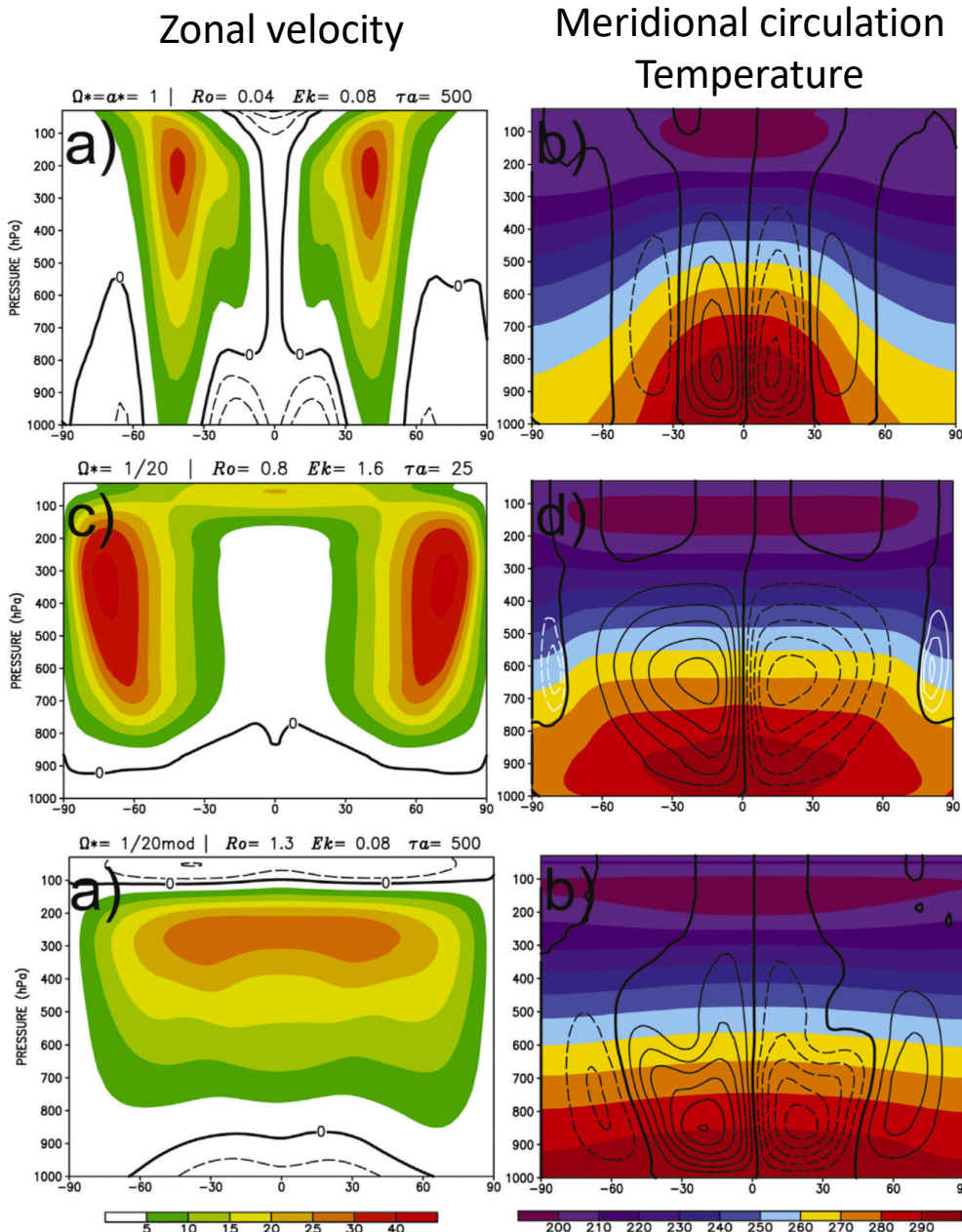


Fig. 3. Meridional distribution of the mean stream function for the MOIST model with $\Omega^* = 0-8$. Units: 10^{13} g s^{-1}

Parameter dependence in an Earth-like GCM

(Dias Pinto & Mitchell 2014)



Earth' condition

$R_o = 0.04$

Rot. rate x 1/20

$R_o = 0.8$

Hadley循環が広がるが、放射・摩擦緩和時間の自転周期に対する比が結果として1/20倍になるためにスーパー口ーテーションにならない

Rot. rate x 1/20

Relaxation time x 20

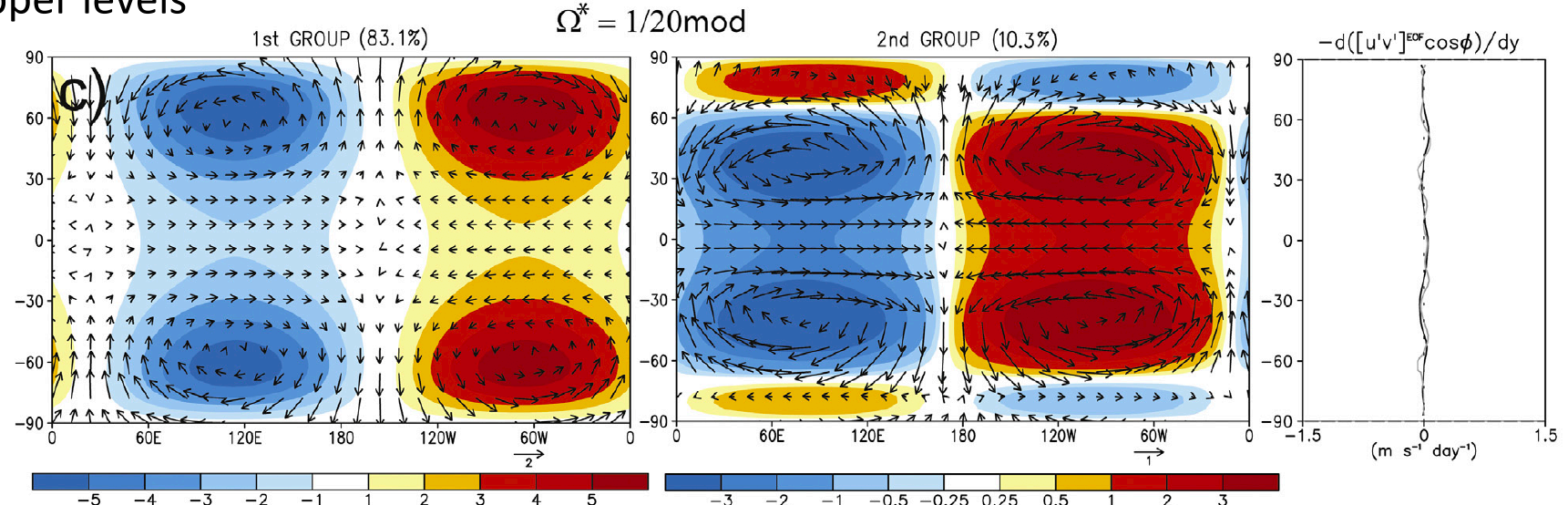
$R_o = 1.2$

放射・摩擦緩和時間を長くするとスーパー口ーテーション

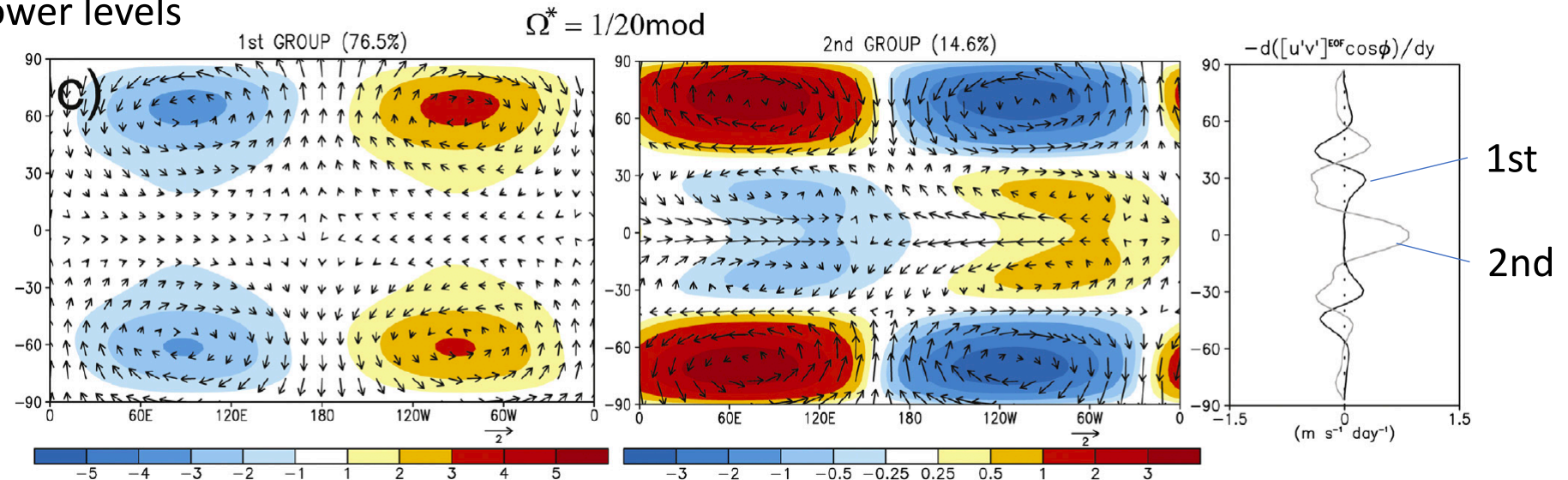
Wave structures (EOF 1, 2)

Rot. rate x 1/20 , Relaxation time x 20

Upper levels

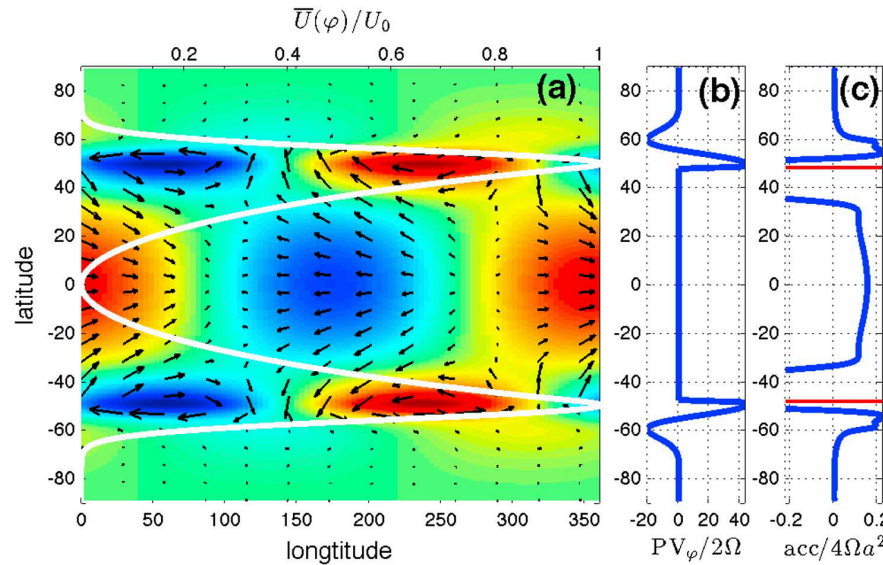


Lower levels

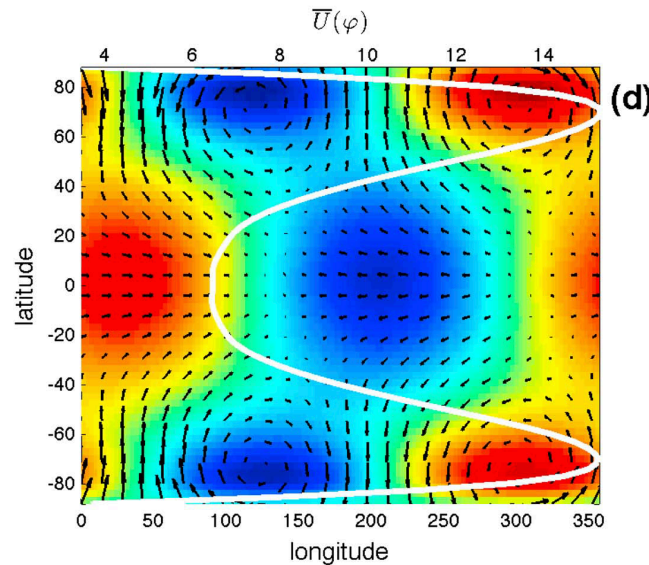


Rossby-Kelvin instability

(Sakai 1989; Iga and Matsuda 2005; Wang & Mitchell 2014)



Linear analysis



Titan-like simulation

Wang & Mitchell (2014)

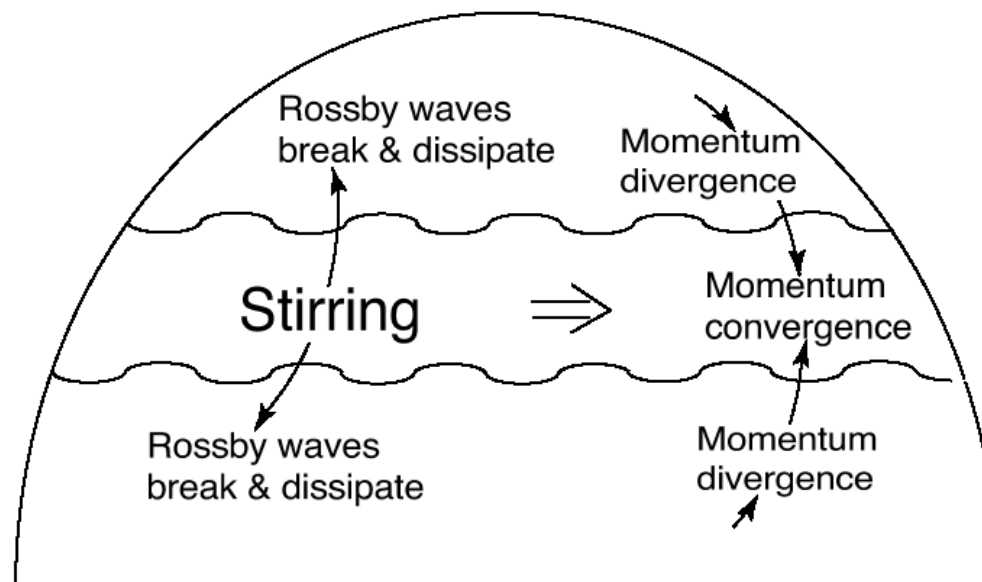
wave momentum transport sustaining Earth's jets

baroclinic instability

→ generation of Rossby waves

→ Rossby waves take away retrograde (westward) angular momentum from the md-latitude

→ maintenance of (eastward) mid-latitude jets



(Vallis, 2005)

Rossby radius of deformation

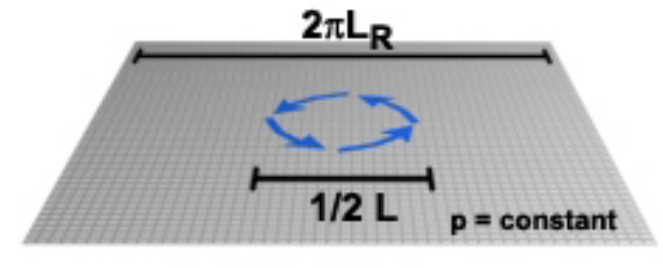
$$L_R = \frac{\sqrt{gH}}{f}$$

g : gravitational acceleration

H : depth of the system

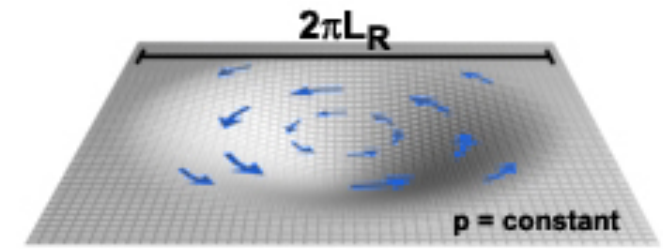
$f = 2\Omega \cos \theta$: Coriolis parameter

The characteristic scale at which the velocity field and the pressure field adjust with each other to maintain geostrophic flow



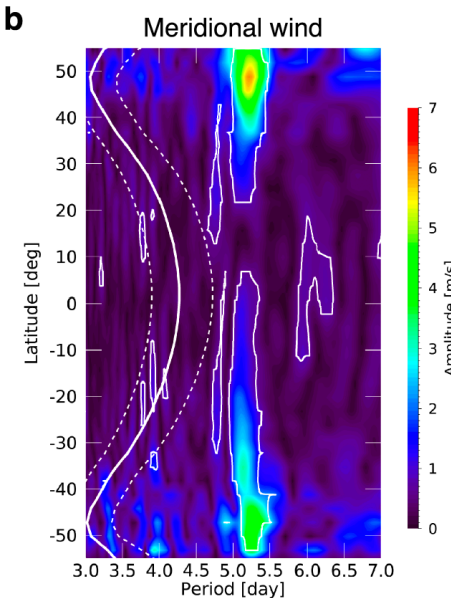
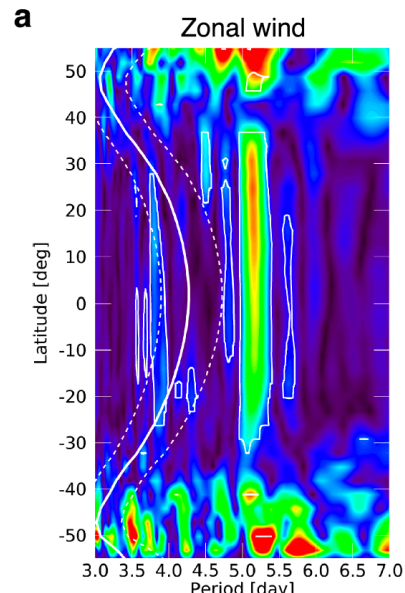
Initial disturbance

Faster planetary rotation leads to large f , and then shorter L_R

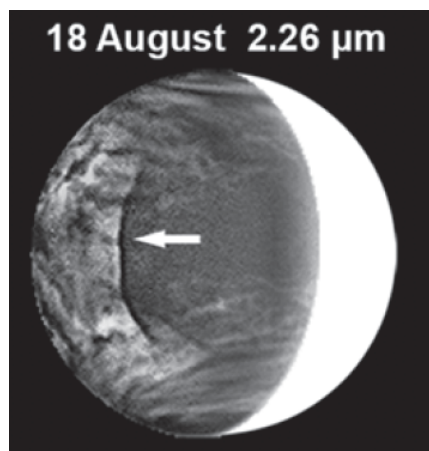


Final adjusted state

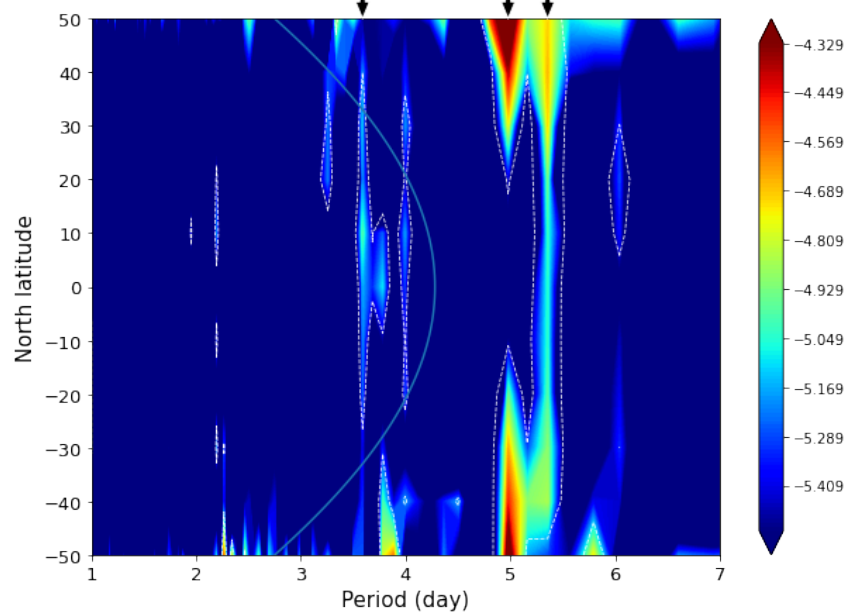
あかつきがとらえた金星大気の惑星規模振動



紫外雲追跡風のスペクトル解析
Imai et al. (2019)

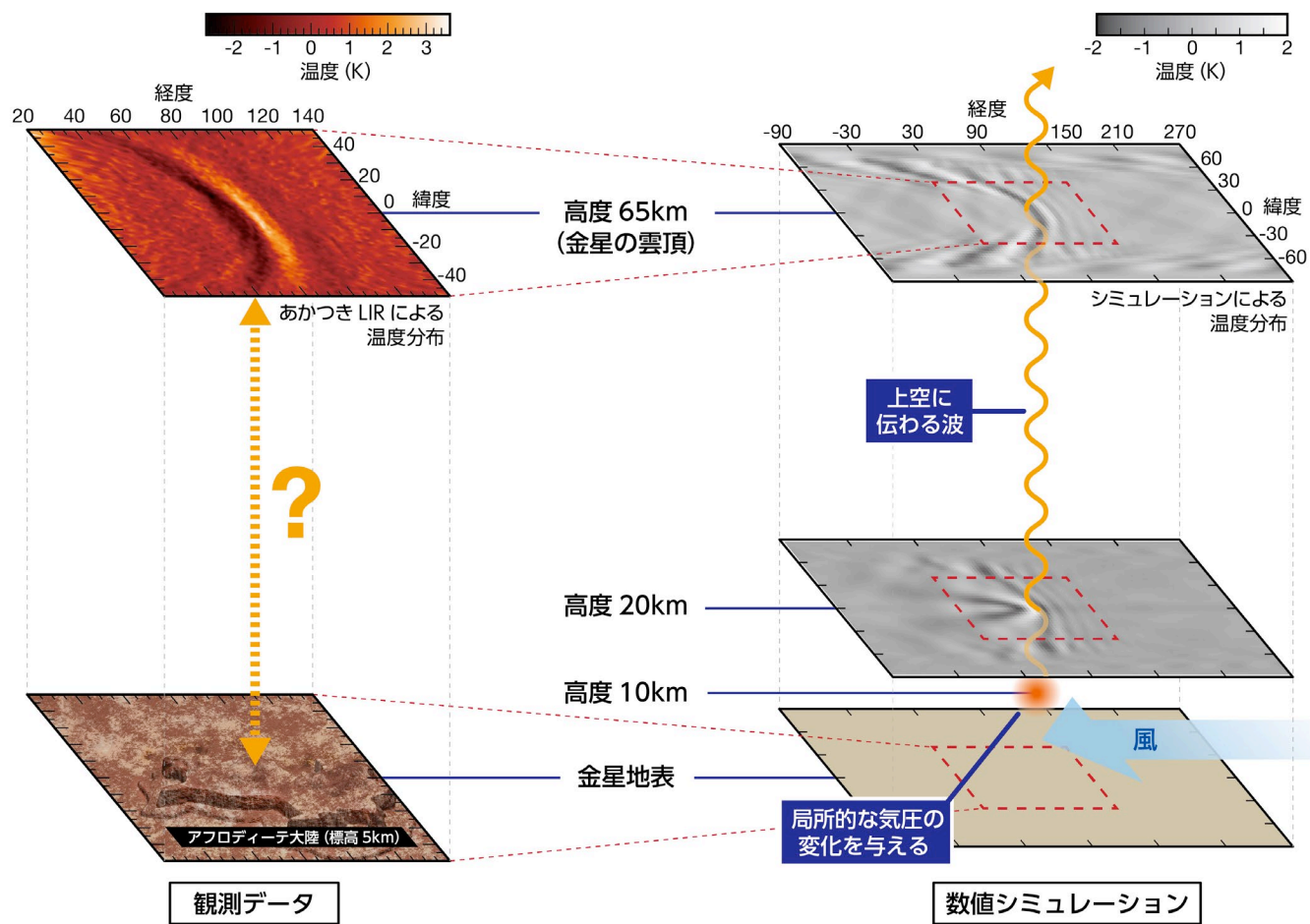
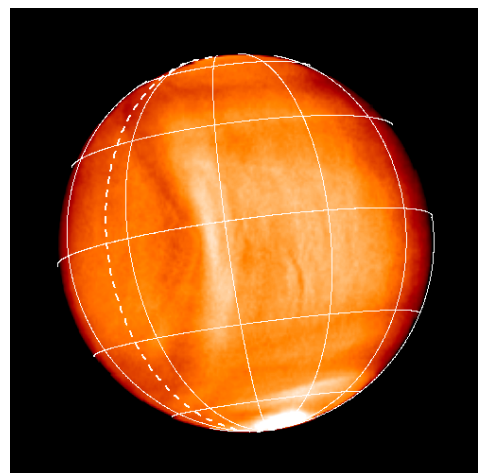


周期5日で伝播する
巨大不連続構造
Peralta et al. (2020)

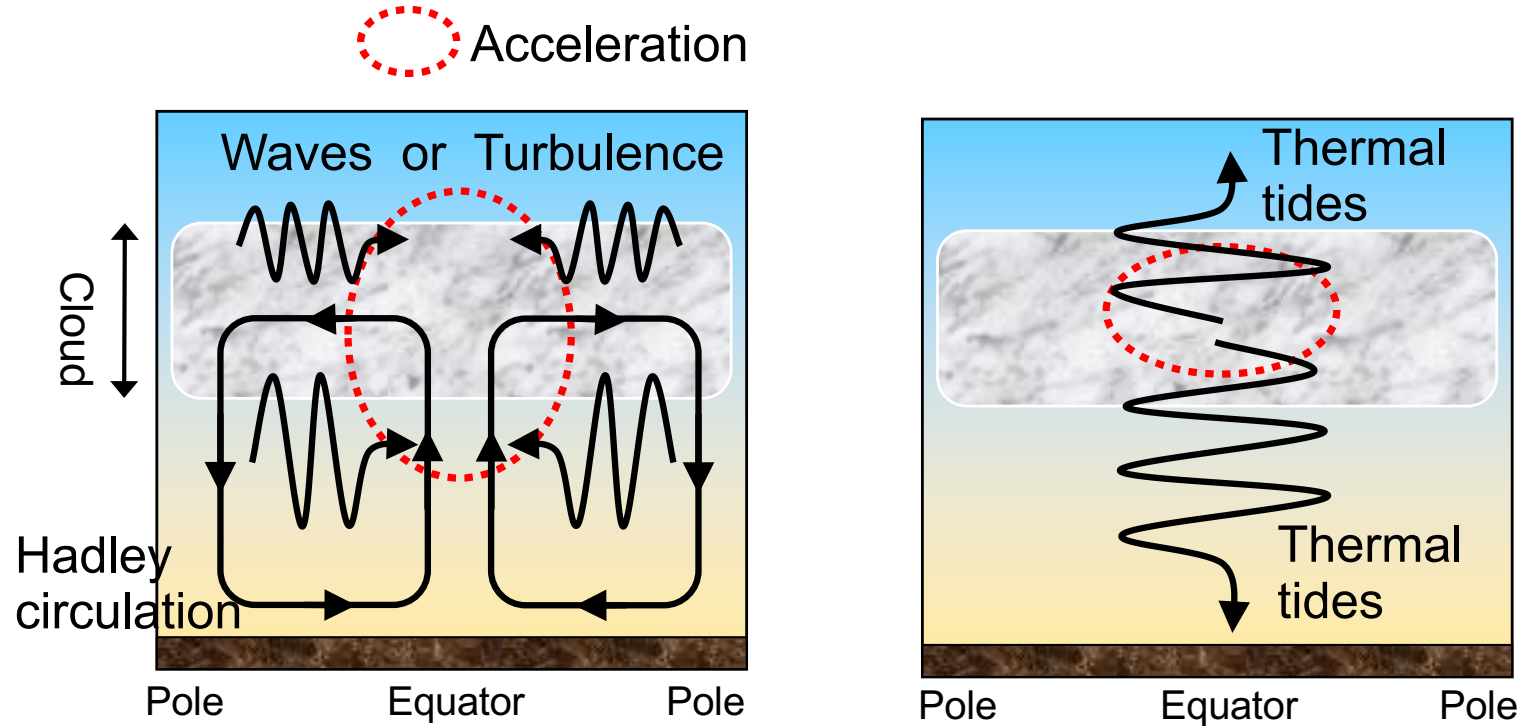


雲頂温度のスペクトル解析
Kajiwara et al. (投稿準備中)

あかつきで見つかった地形性重力波の不思議

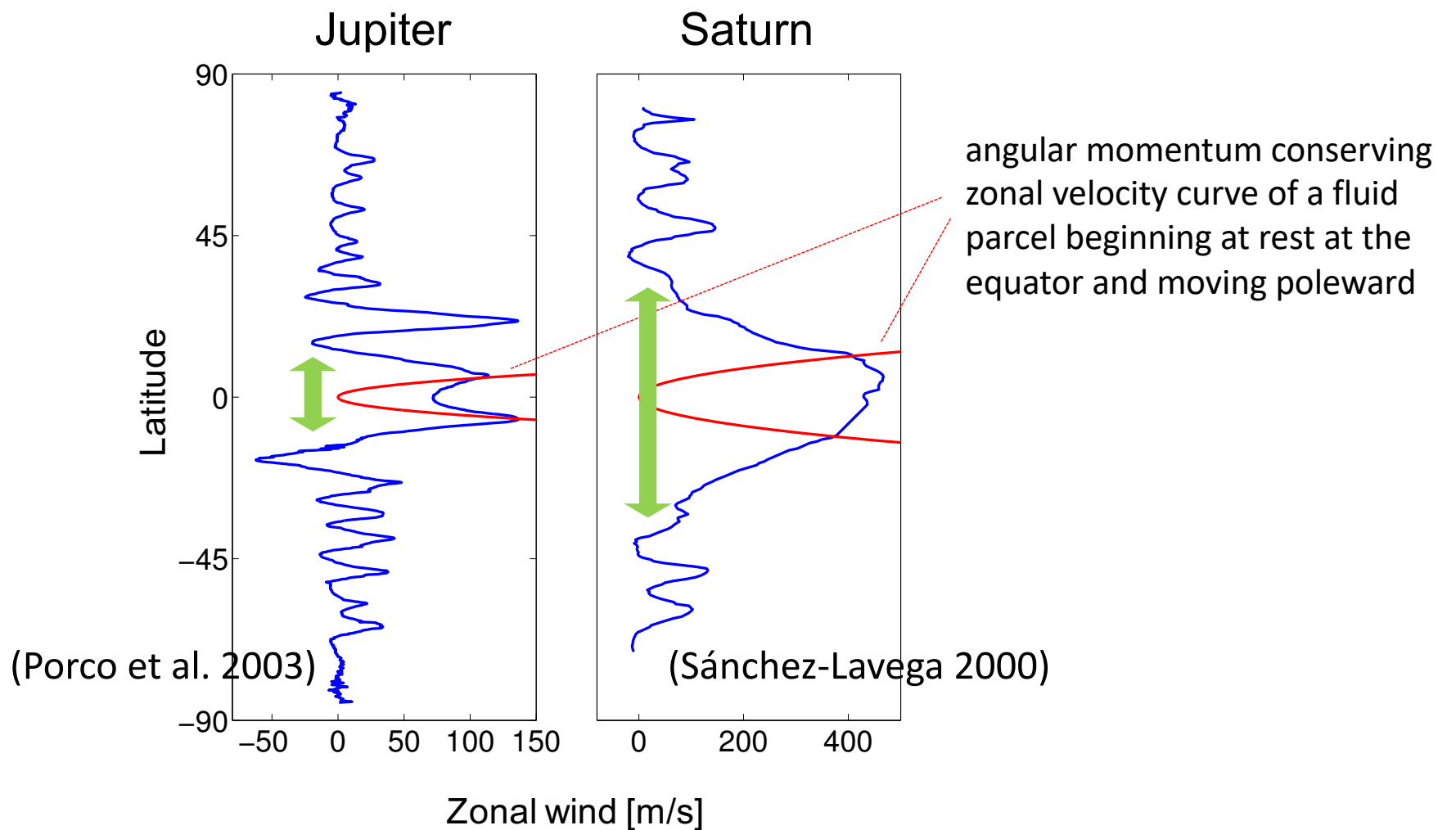
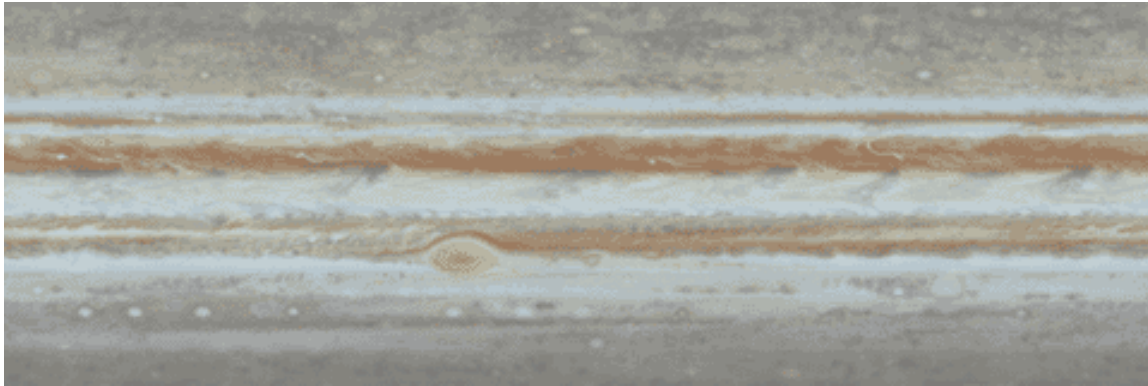


下層大気の風？



- どちらのメカニズムにしても赤道域の大気最下層ではスーパーローーションとは逆向きの流れを期待（そのことによって固体部分から大気へ角運動量を受け渡す）
- 地形性重力波が上空まで伝わるには全高度でスーパーローーション方向の流れでなくてはならない

Superrotation on the gas giants

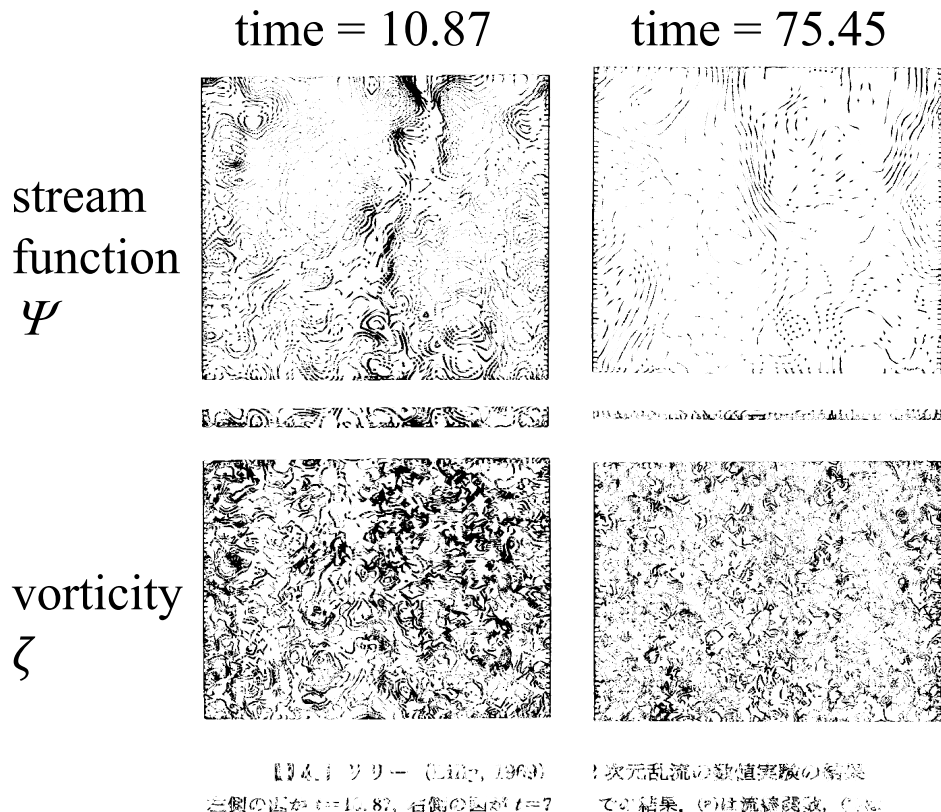


Modeling Jupiter and Saturn's zonal flows

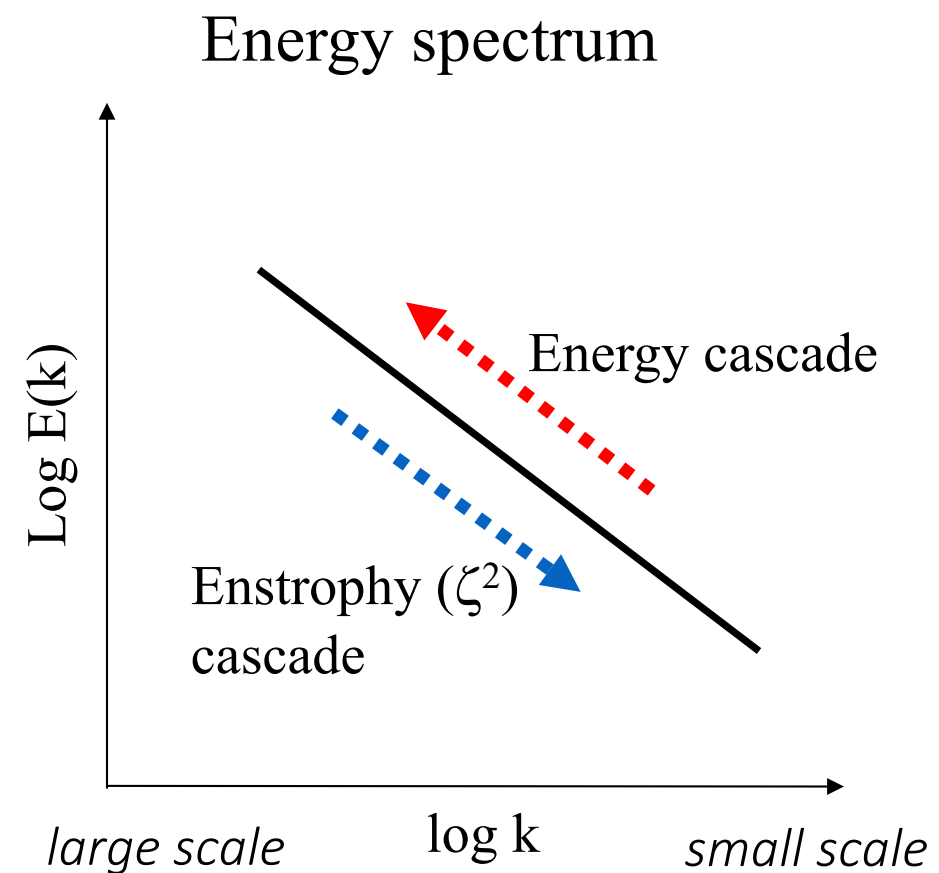
- Shallow models
 - The dynamics are shallow, such as on a terrestrial planet
 - The strong east-west flows can result from 2D geostrophic turbulence and/or baroclinic instability
- Deep models
 - the observed jets are the surface manifestation of convective columns originating from the hot interiors

Two-dimensional turbulence

- Small eddies tend to organize large eddies as time passes
- Turbulent energy cascade toward large scales (smaller wavenumber k)



Lilly (1969)



Rhines scale

- Vorticity equation

$$\left(\frac{\partial}{\partial t} + \vec{v}_g \cdot \nabla \right) (\zeta_g + f) = 0$$

$$\frac{\partial \zeta}{\partial t} + u \frac{\partial \zeta}{\partial x} + v \frac{\partial \zeta}{\partial y} + \beta v = 0$$

nonlinear term beta effect
= origin of = origin of
turbulence Rossby wave

Φ : geopotential

β : df/dy

U : typical velocity

$k^2 U^2 > \beta U$: turbulence

$k^2 U^2 < \beta U$: Rossby wave

- Rhines scale

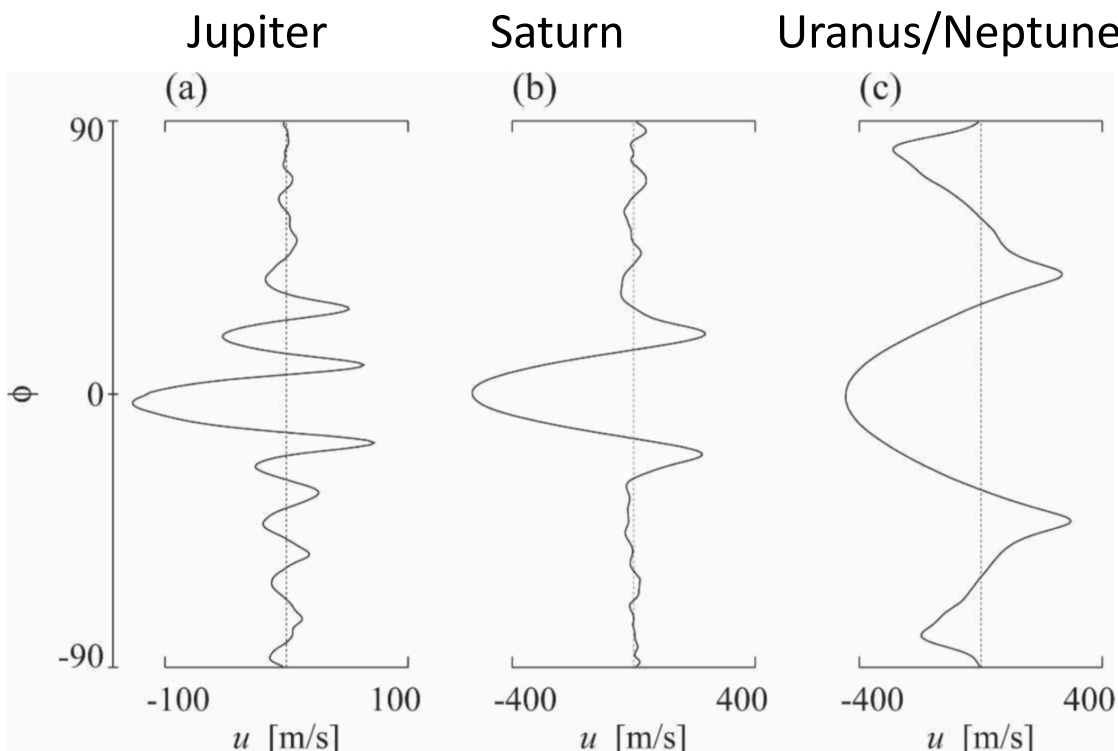
$$k_\beta = \sqrt{\frac{\beta}{U}}$$

Upward cascade of turbulence energy stops at smaller scales ($k < k_\beta$)

Shallow-water turbulence on the sphere of the giant planets

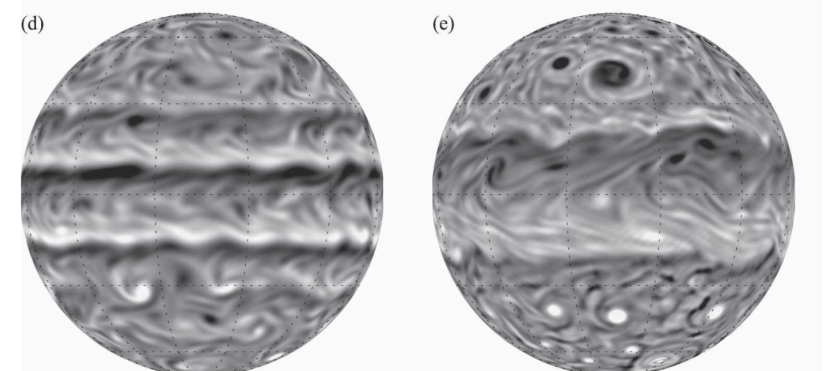
- Forcing are given to the vorticity field as a small-scale, random process, or eddies are generated by baroclinic instability
- Inverse energy cascade generates multiple jets on the order of the Rhines scale
- The simulated equatorial flow is mostly retrograde

Zonal velocity



Scott & Polvani (2007)

Vorticity field

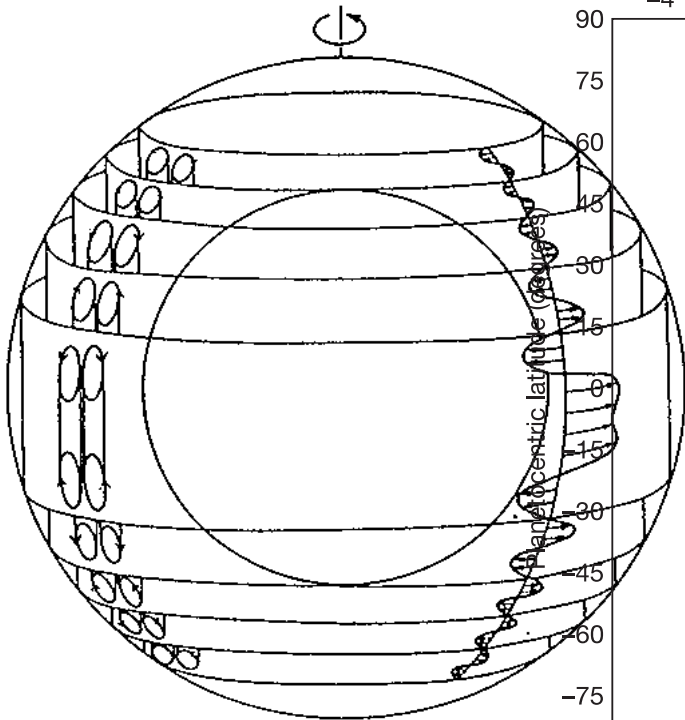


Jupiter ($Ro=0.002$)

Saturn ($Ro=0.013$)

Taylor–Proudman theorem

- In a fluid that is steadily rotated, the fluid velocity will be uniform along any line parallel to the axis of rotation.



Momentum equation in rotational frame

$$\frac{d\vec{v}}{dt} + 2\vec{\Omega} \times \vec{v} + \frac{1}{\rho} \nabla p + \nabla \Phi = 0$$

Assuming non-compressivity and $d/dt=0$,
the curl is applied to give

$$\vec{\Omega} \cdot \nabla \vec{v} = 0$$

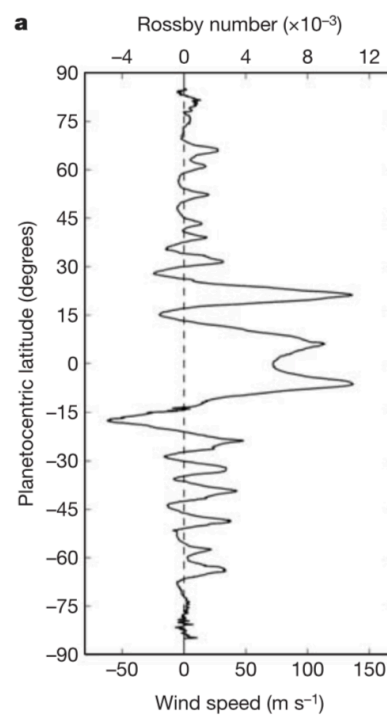
Taking z-axis along the planet's rotational axis,

$$\frac{\partial \vec{v}}{\partial z} = 0$$

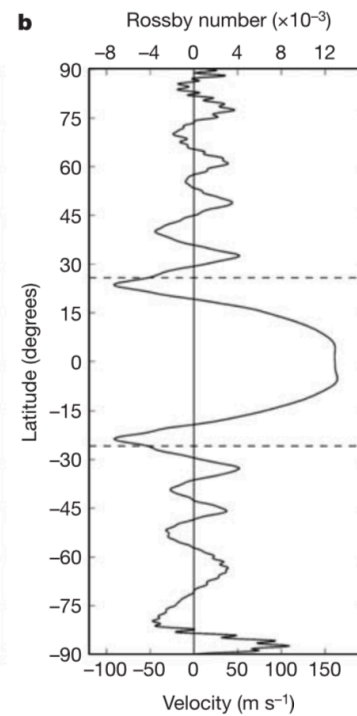
Busse (1994)

Deep models

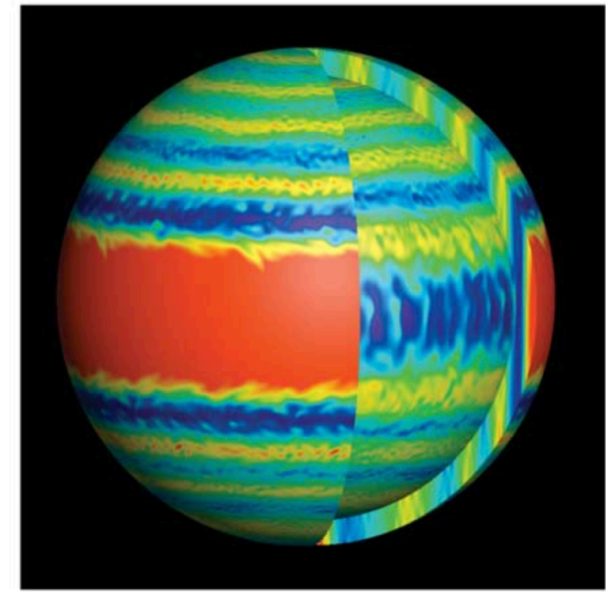
Observation



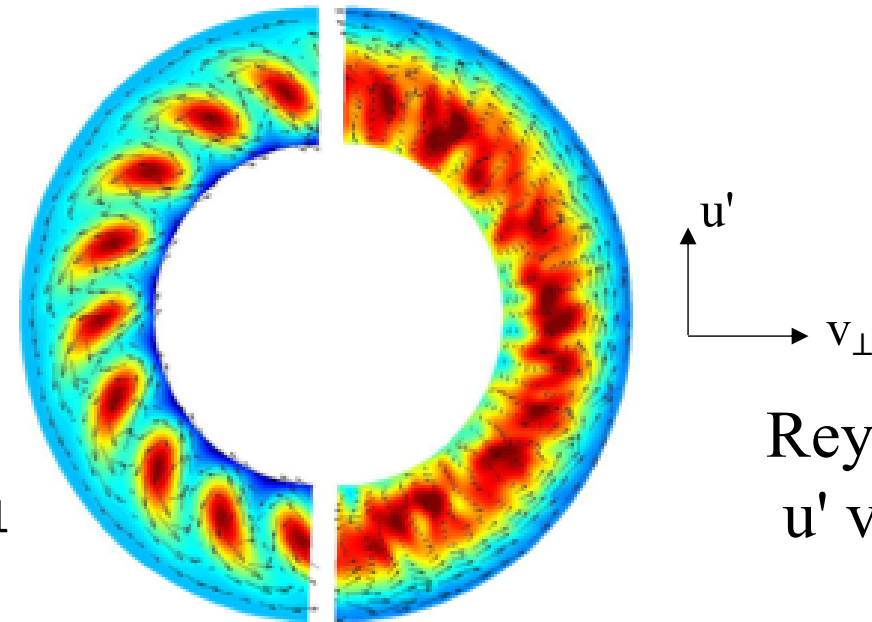
Model



Zonal velocity



Heimpel et al. 2005



Showman et al. 2011

Reynolds stresses
 $u' v_{\perp}' > 0$

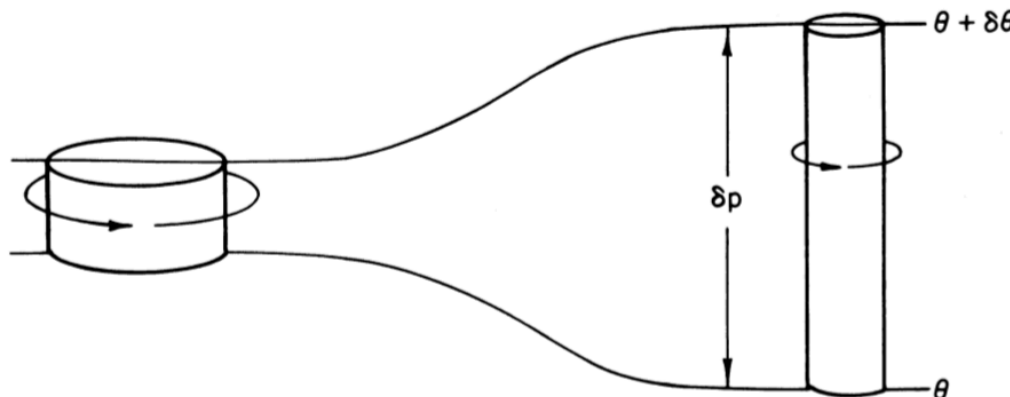
Quasi-geostrophic vorticity equation

$$\frac{\partial \zeta_g}{\partial t} = -\vec{v}_g \cdot \nabla(\zeta_g + f) + f_0 \frac{\partial \omega}{\partial p}$$

$$\zeta_g \equiv \frac{\partial v_g}{\partial x} - \frac{\partial u_g}{\partial y} = \frac{\nabla^2 \Phi'}{f_0} \quad : \text{geostrophic vorticity}$$

Vorticity changes with time through

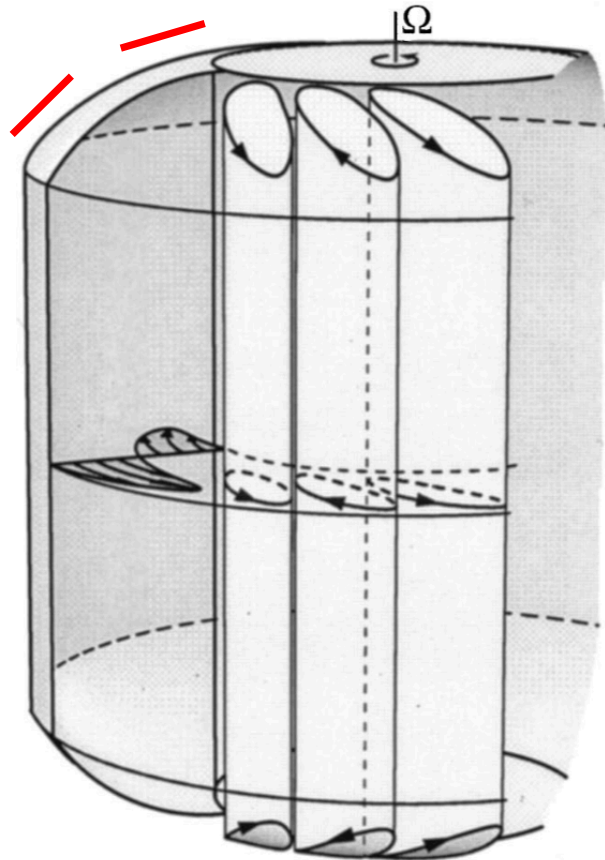
- advection of absolute vorticity ($\zeta_g + f$) by geostrophic wind (\vec{v}_g)
- vertical divergence (horizontal divergence)



Holton (2004)

Fig. 4.7 A cylindrical column of air moving adiabatically, conserving potential vorticity.

Thermal Rossby wave



Busse (2002)

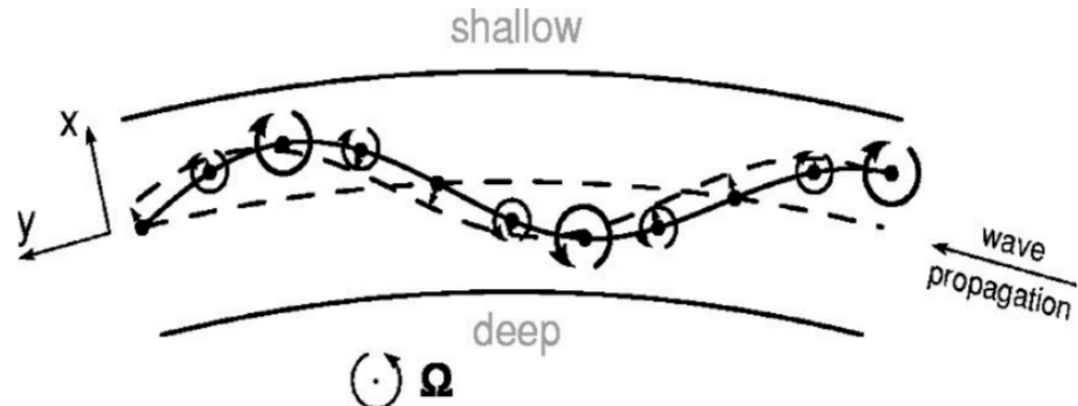
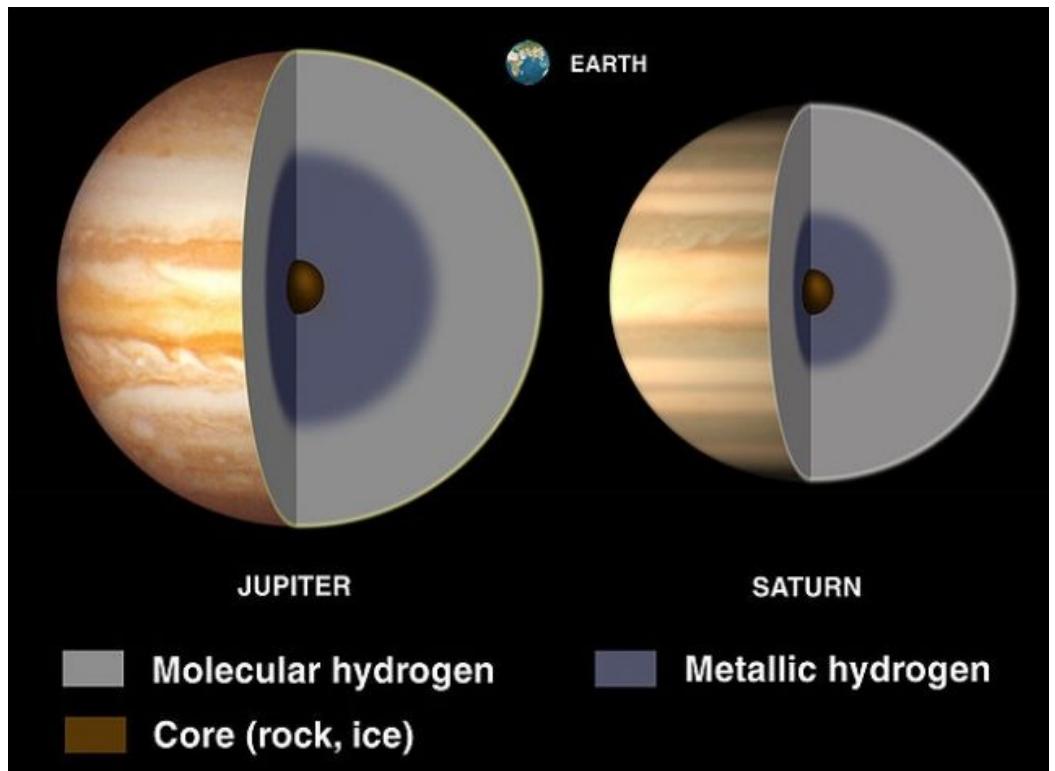
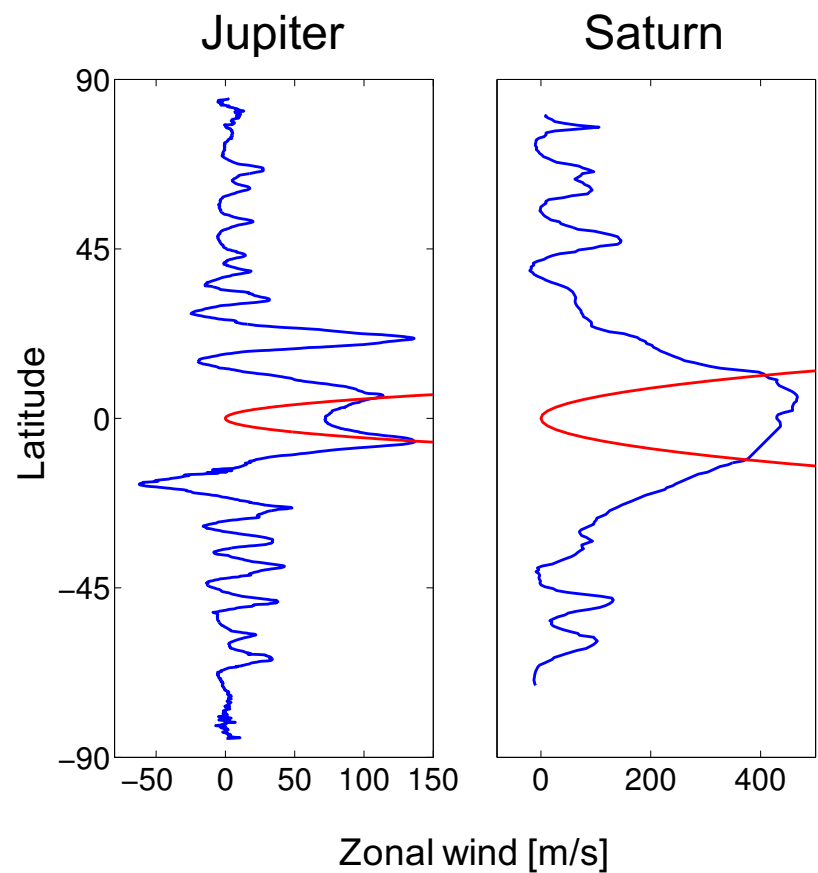


FIG. 2. The mechanism of propagation of a Rossby wave visualized in the equatorial plane of the rotating annulus: Fluid columns originally resting at the mid-surface acquire anticyclonic vorticity relative to the rotating system when they are displaced outwards towards the shallow region. Cyclonic vorticity is acquired by the displaced columns inwards. The action of the columnar motion on the neighboring fluid columns is such that an initial sinusoidal displacement propagates in the prograde direction.

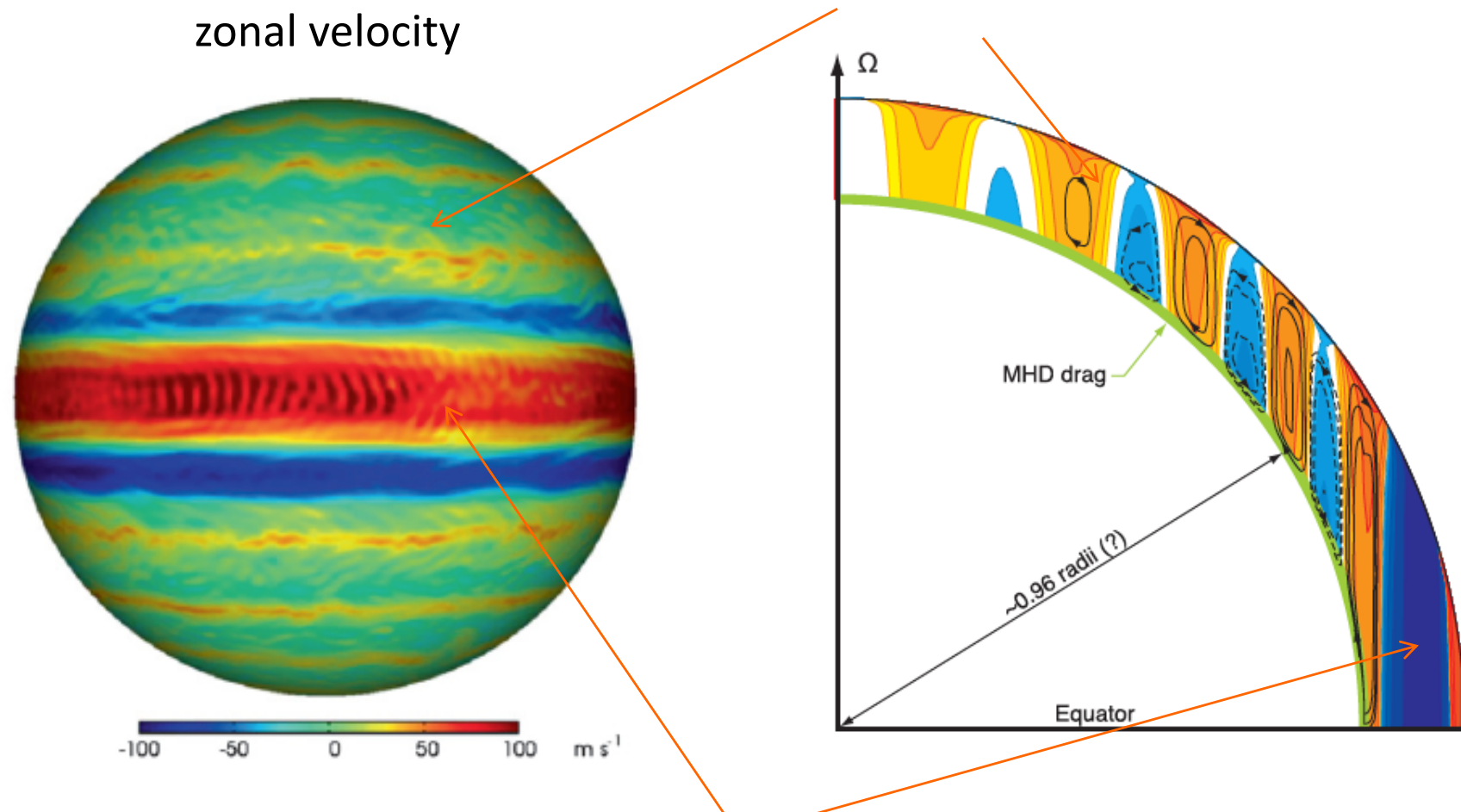
The columns are tilted because the thermal Rossby wave has the tendency to propagate faster on the outside than on the inside. A prograde differential rotation on the outside with a retrograde one near the inner cylinder must thus be expected.



from Wikipedia

Schneider & Liu (2009)

中・高緯度では太陽光加熱の緯度による違いによって傾圧不安定が生じ、ここから放射されるロスビー波に伴う運動量収束・発散によって西風や東風のジェットが作られる。

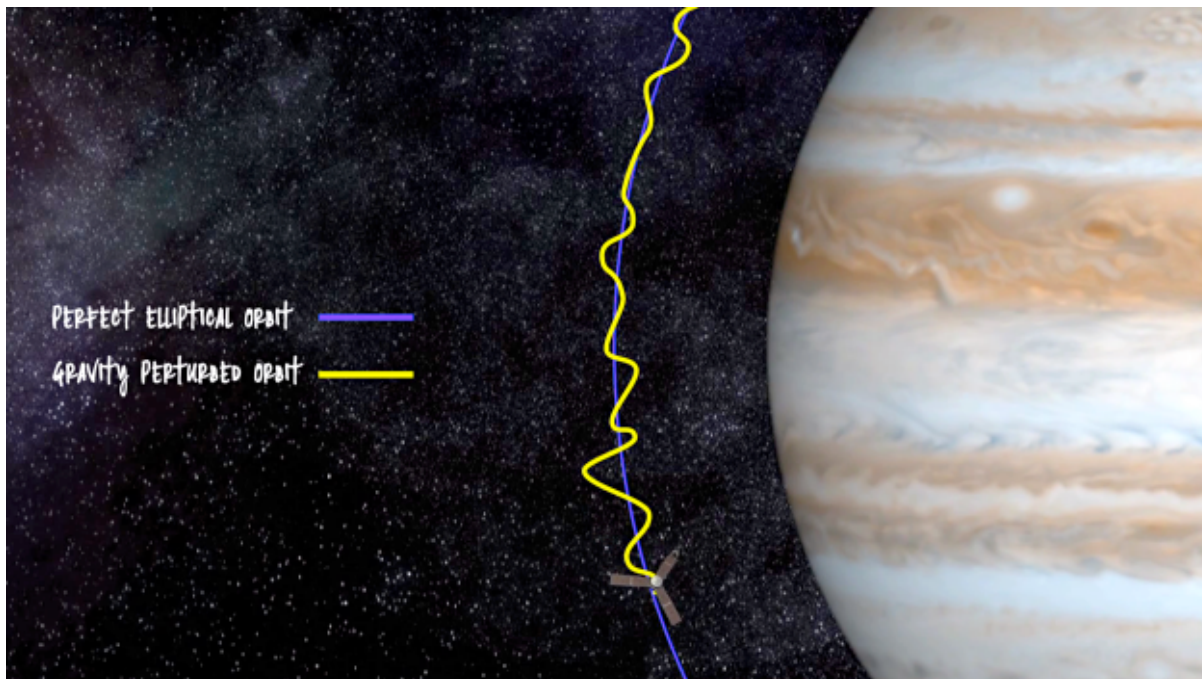


赤道では深部からの熱フラックスにより対流が生じ、ここからロスビー波が高緯度に向けて放射される結果、運動量が収束して赤道ジェットが作られる。

Doppler tracking of Juno spacecraft

Less et al. (2018)

- The spacecraft acts as a test particle falling in the gravity field of the planet. Jupiter's gravity is inferred from range-rate measurements between a ground antenna and the spacecraft during perijove passes.
- The ground station transmits carrier signals, and the on-board translator lock the incoming carrier signals and retransmit them back to the ground. The range-rate (Doppler) observable is obtained by comparing the transmitted and received frequencies.
- Spherical harmonics representation of planetary gravity fields is determined by the density distribution inside the body.



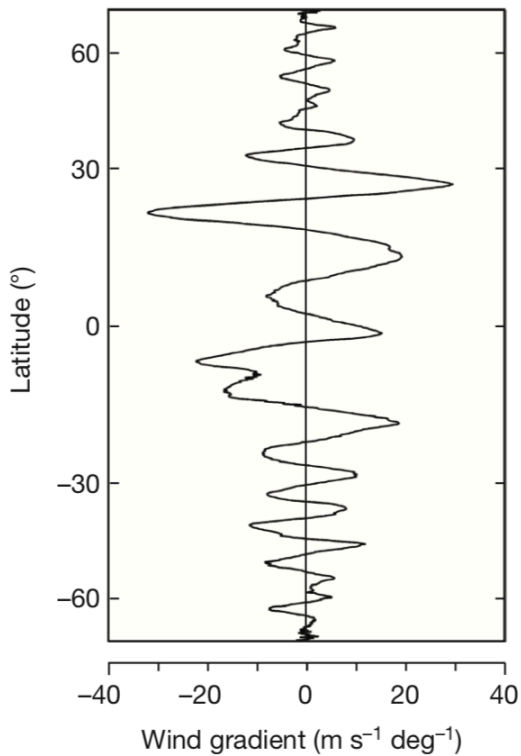
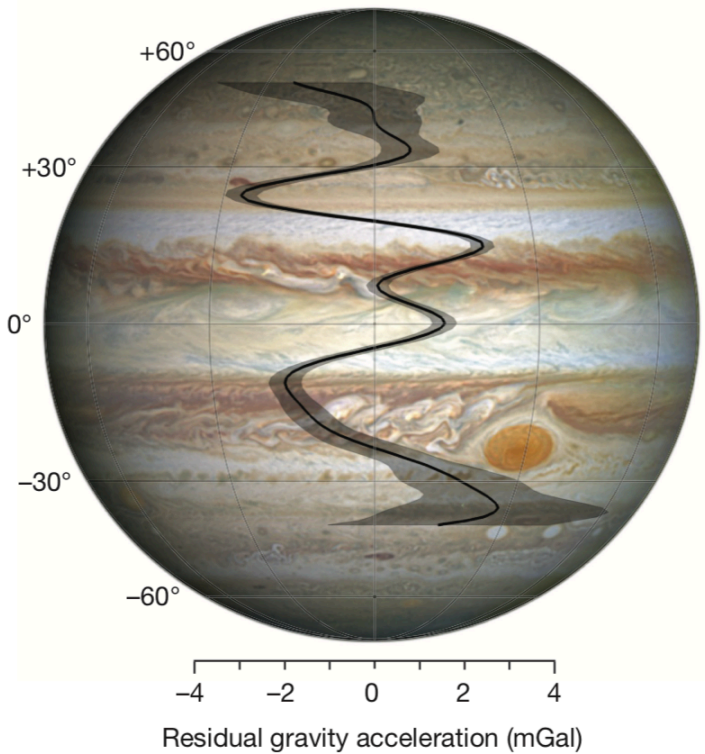
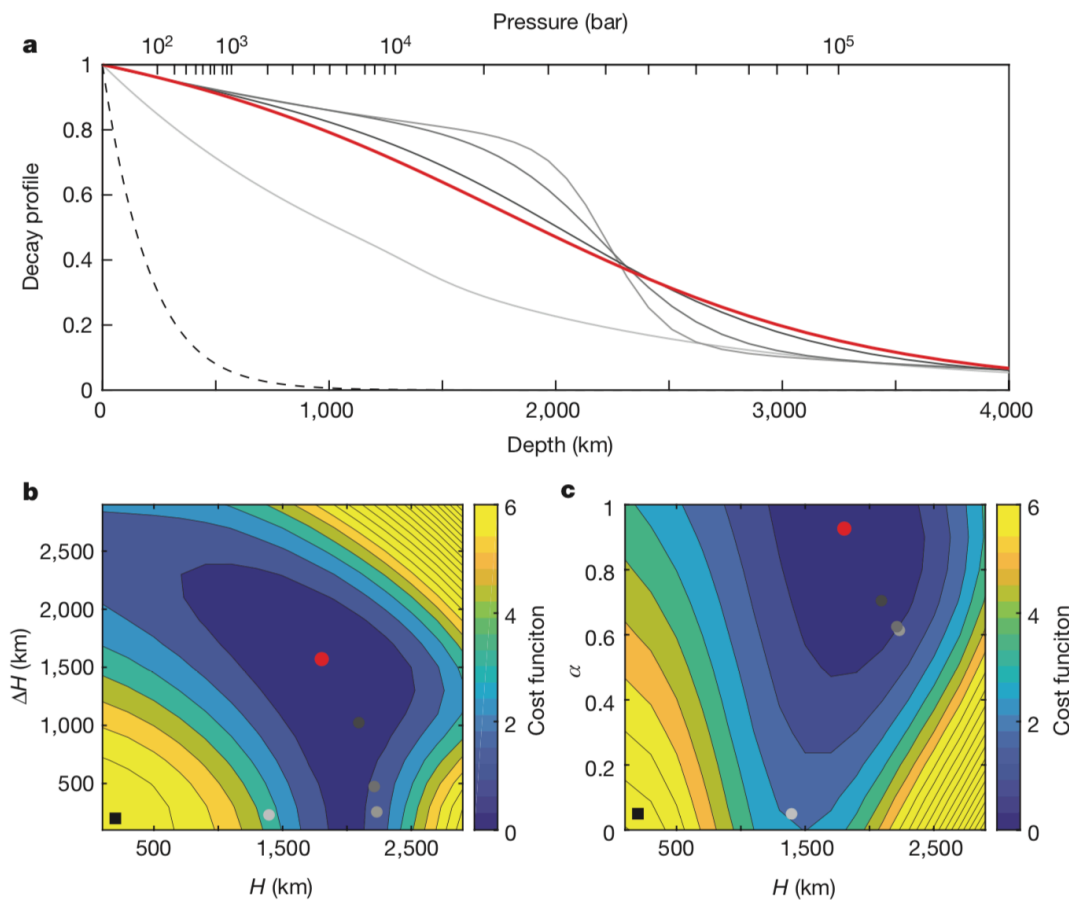
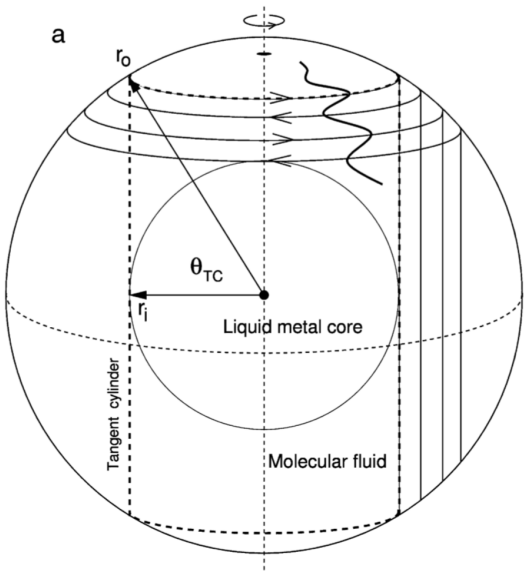


Figure 3 | Gravity disturbances due to atmospheric dynamics. **a**, An image of Jupiter taken by the Hubble Wide Field Camera in 2014 (<https://en.wikipedia.org/wiki/Jupiter>), showing the latitudinal dependence of residual gravity acceleration (in milligals, positive outwards) and associated 3σ uncertainty (shaded area) at a reference distance of 71,492 km, when the gravity from the even zonal harmonics J_2 , J_4 , J_6 and J_8 is removed. The residual gravity field, which is dominated by the dynamics of the flows, shows marked peaks correlated with the band structure. **b**, Latitudinal gradient of the measured wind profile. The largest (negative) peak of $-3.4 \pm 0.4 \text{ mGal}$ (3σ) is found at a latitude of 24° N, where the latitudinal gradient of the wind speed reaches its largest value. The relation between the gravity disturbances and wind gradients is discussed in an accompanying paper⁴.

Less et al. (2018)



$$u(r, \theta) = u_{\text{cyl}}(s)Q(r) \quad (12)$$

where $u_{\text{cyl}}(s)$ is the cloud-level azimuthal wind projected downward along the direction of the axis of rotation, and $s = r\cos(\theta)$ is the distance from the axis of rotation. $Q(r)$ is the radial decay function we optimize, given by

$$Q(r) = (1 - \alpha)\exp\left(\frac{r - a}{H(\theta)}\right) + \alpha \left[\frac{\tanh\left(-\frac{a - H(\theta) - r}{\Delta H}\right) + 1}{\tanh\left(\frac{H(\theta)}{\Delta H}\right) + 1} \right] \quad (13)$$

where a is the planetary radius, α is the contribution ratio between an exponential and a normalized hyperbolic tangent function and ΔH is the width of the hyperbolic tangent. We take a hierarchical approach using this profile at several levels of

Kaspi et al. (2018)

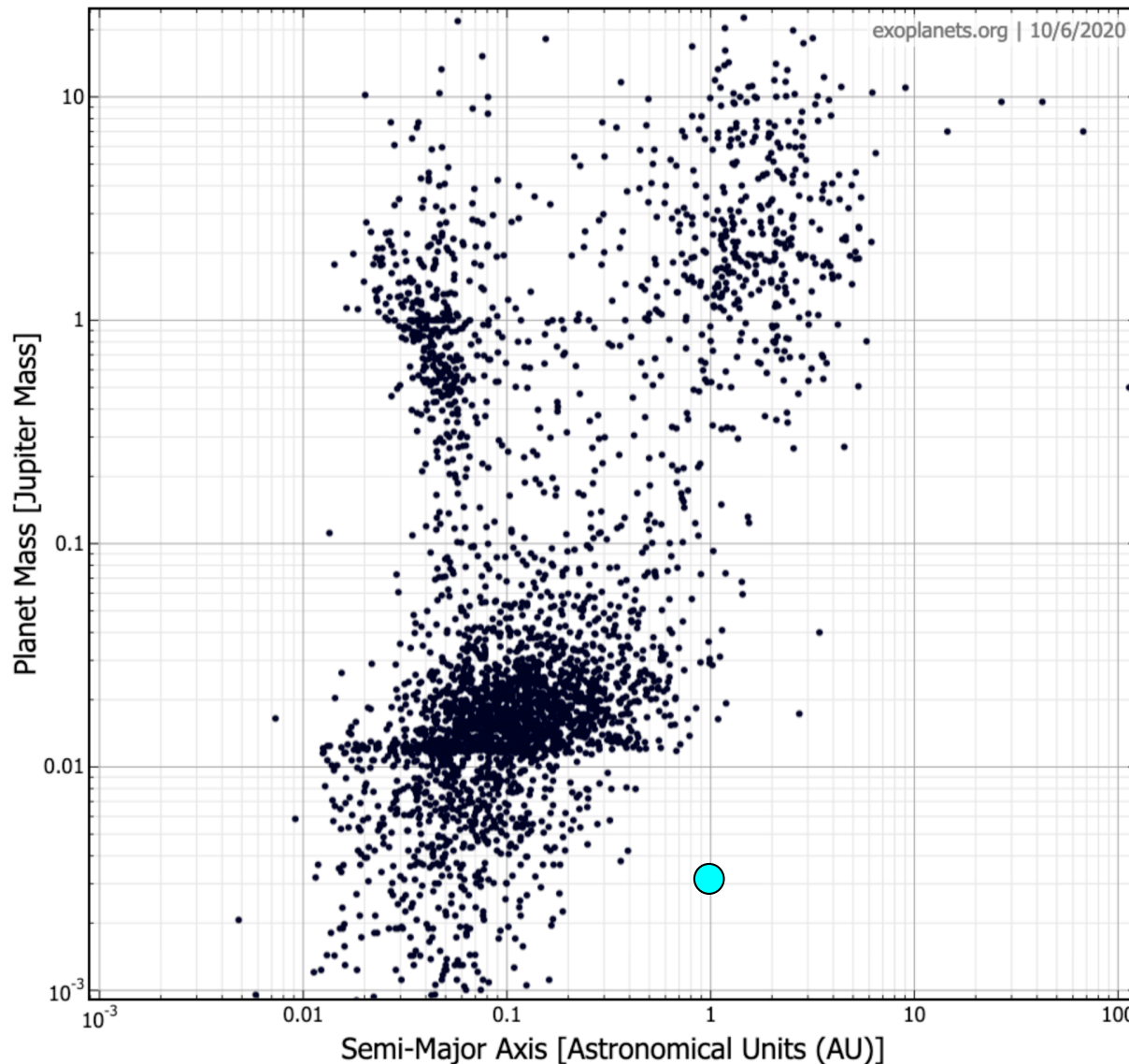
The observed jet streams, as they appear at the cloud level, extend down to depths of thousands of kilometres beneath the cloud level, probably to the region of magnetic dissipation at a depth of about 3,000 kilometres

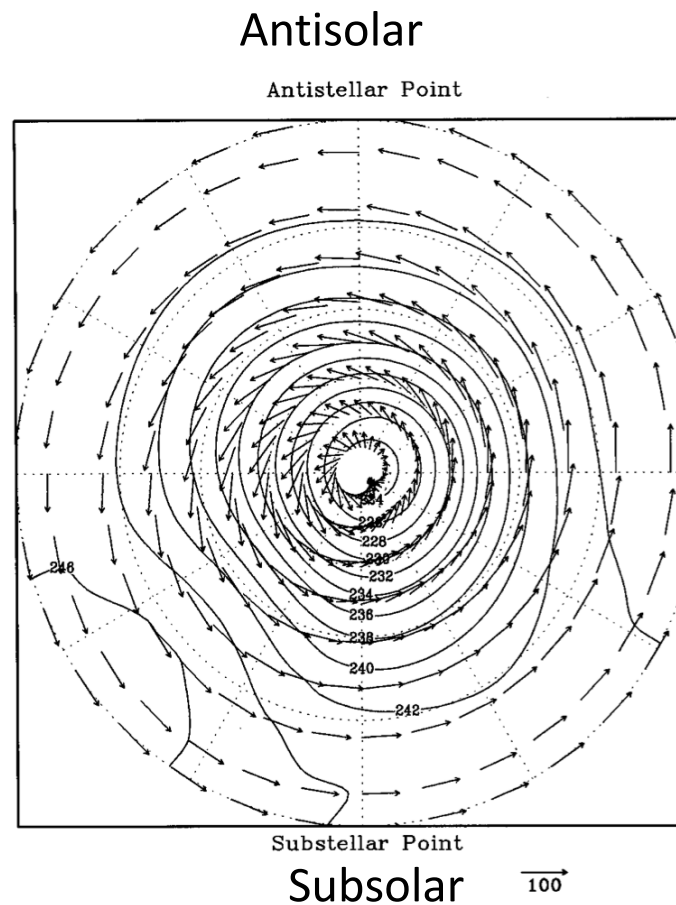
木星-土星比較

- JunoとCassini の重力計測によれば土星のジェットは木星に比べて3倍の深さまで及んでいる(3000 km on Jupiter and 9000 km on Saturn). これは大気が導電性を持ちオーム抵抗が生じる深さに対応すると考えられる。
- 赤道スーパーローーションの到達緯度は木星では 13° 、土星で 31° くらい。これは導電性が生じる深さから自転軸方向に伸ばした直線が表面と交わるあたりに相当する。
- スーパーローーションメカニズムはまだ同定されていない

Exoplanets

中心星近傍をまわる惑星 = 同期回転(潮汐固定)？

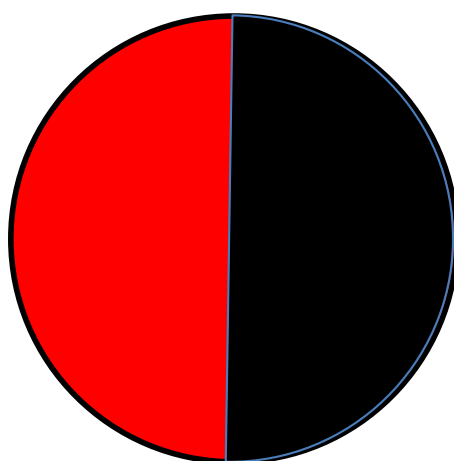




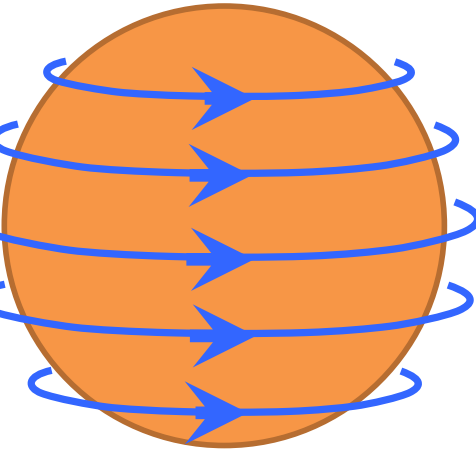
Polar view of the atmospheric circulation and temperature distribution at 20 km altitude on a synchronously rotating terrestrial planet (Joshi et al., 1997)

Implications for exoplanets' environments

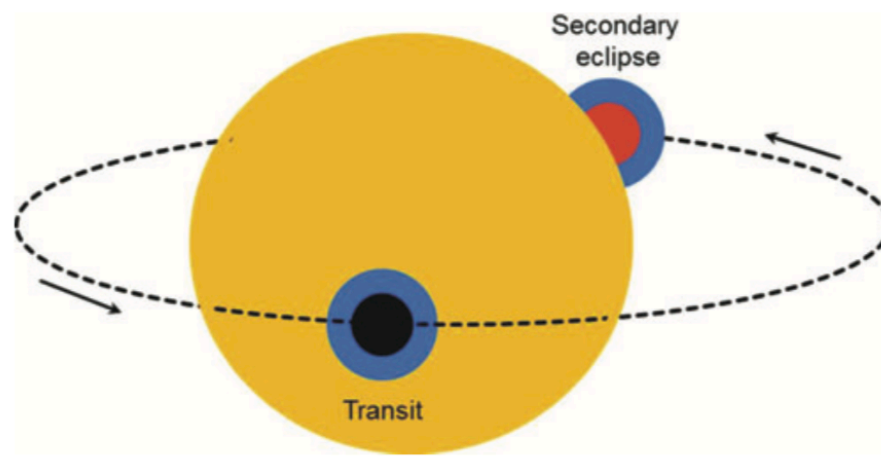
Tidally-locked planets are mostly slow rotators like Venus. Super-rotation can redistribute thermal energy along the local time on such planets.



**Hot dayside
Cold nightside**



Moderate climate?

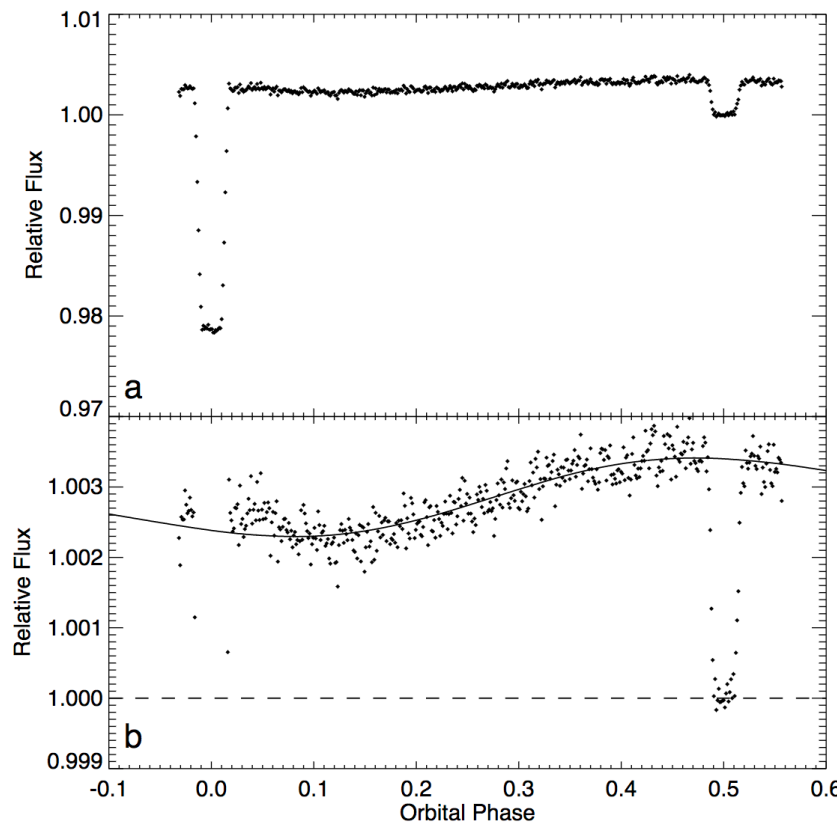


Lammer et al. (2013)

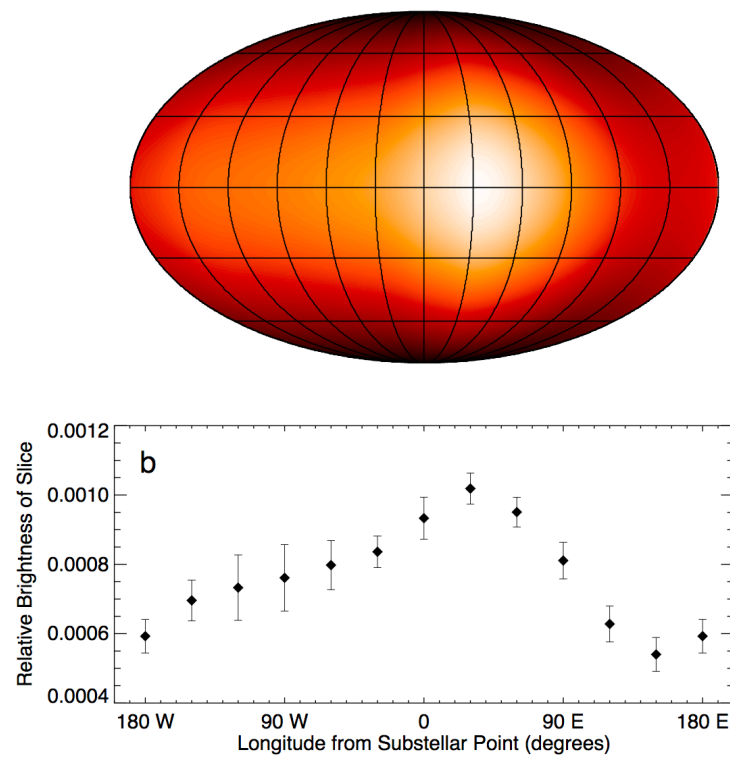
Day-night temperature contrast of an extrasolar planet (Knutson et al. 2007)

A minimum brightness temperature of 973 ± 33 K and a maximum brightness temperature of 1212 ± 11 K at a wavelength of 8 microns, indicating that energy from the irradiated dayside is efficiently redistributed throughout the atmosphere

Observed phase variation for HD 189733b, with transit and secondary eclipse visible.

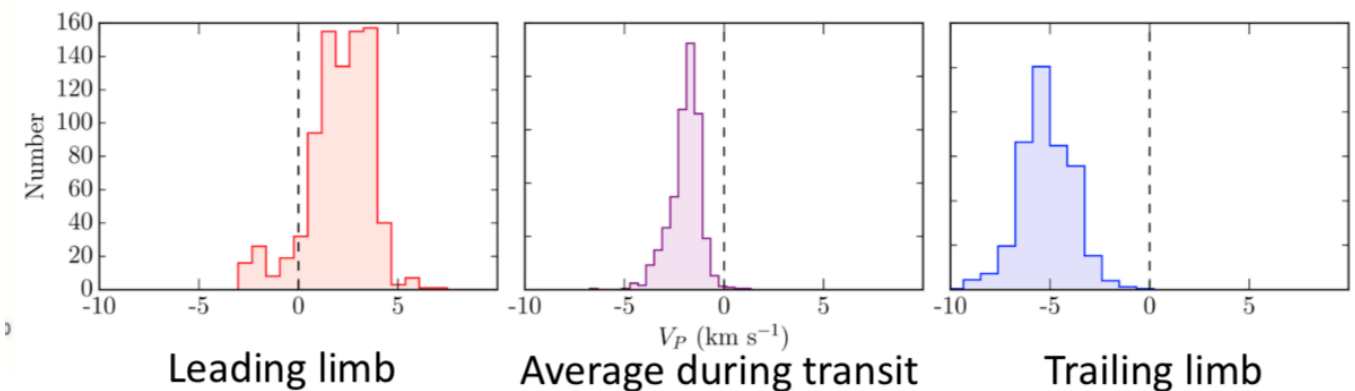
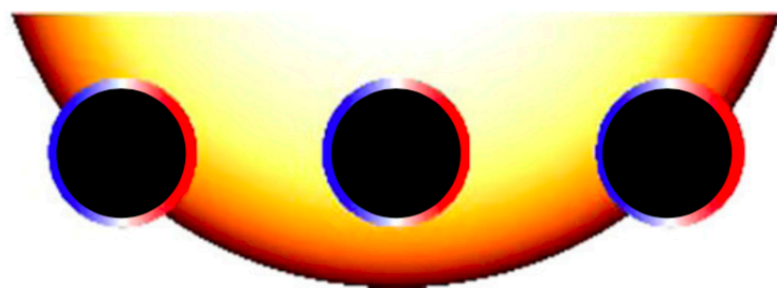


Brightness estimates for 12 longitudinal strips on the surface of the planet



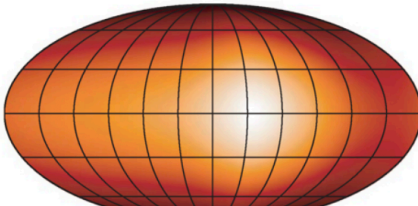
Doppler measurements at the planetary limb during transit (Louden & Wheatley 2015)

- Doppler measurements on opposite sides of the hot Jupiter HD 189733b using sodium absorption in high-resolution transmission spectra
- A redshift of 2.3 km s^{-1} on the leading limb of the planet and a blueshift of 5.3 km s^{-1} on the trailing limb
- These velocities can be understood as a combination of tidally locked planetary rotation and an eastward equatorial jet

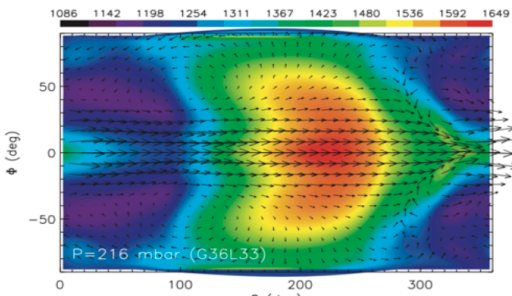


Numerical models of hot Jupiters

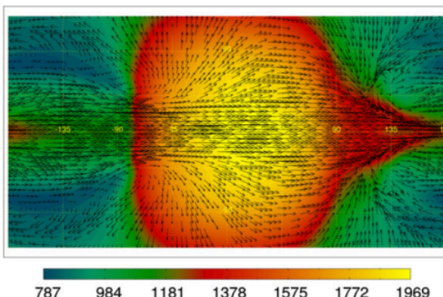
Showman et al. (2020)



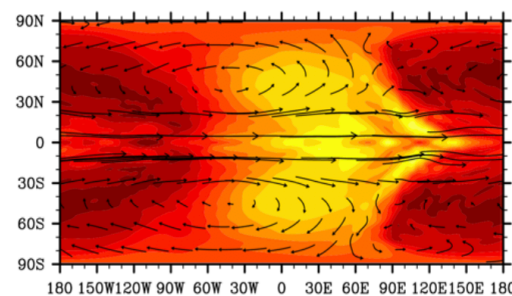
Knutson et al. (2007) (Observation)



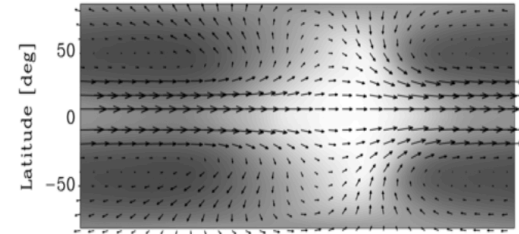
Heng et al. (2011)



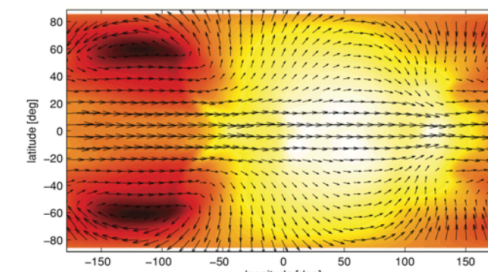
Rauscher & Menou (2012)



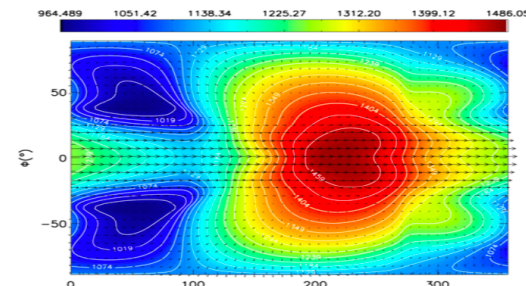
Cho et al. (2015)



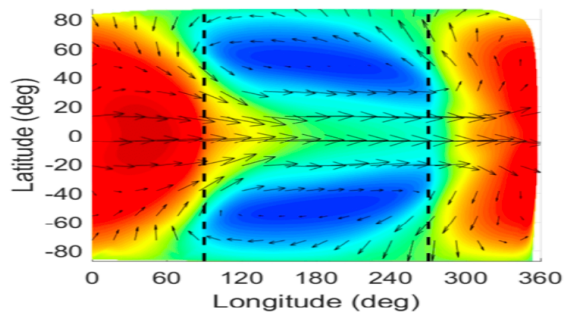
Showman & Guillot (2002)



longitude [deg]



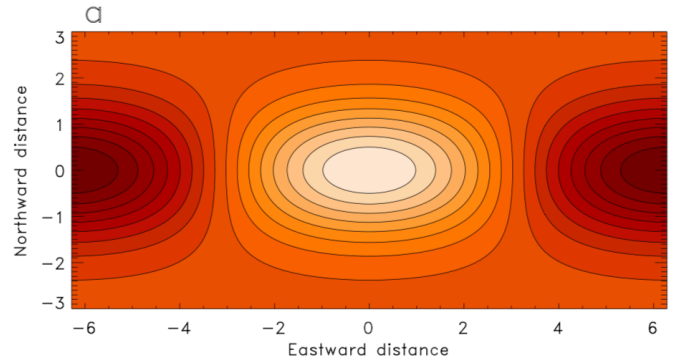
Amundsen et al. (2016)



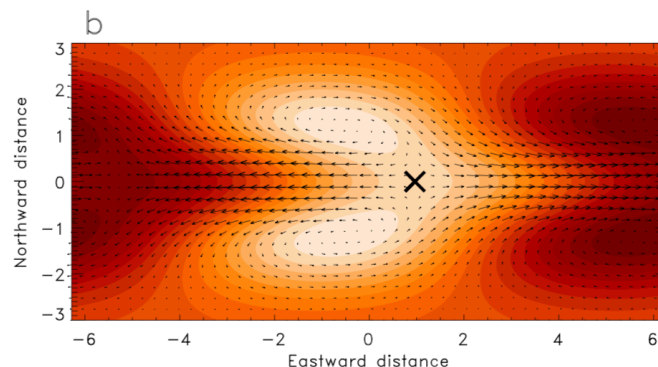
Mendonca et al. (2018)

Linear, analytic solution for parameters relevant to hot, tidally locked exoplanets

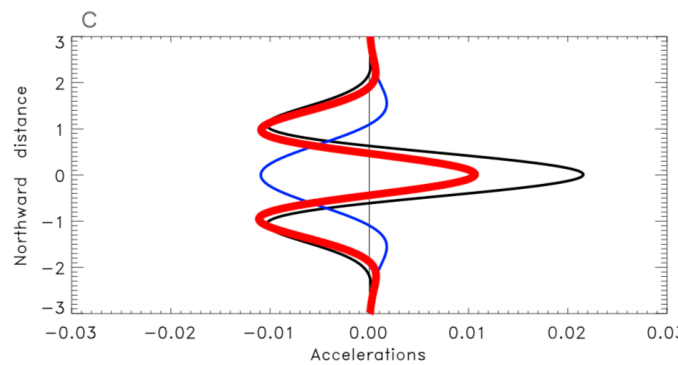
(Showman & Polvani 2011)



radiative-equilibrium height field



Height field (orange scale) and horizontal wind velocities (arrows)



Acceleration

black: meridional momentum convergence
blue: vertical momentum convergence
red: net acceleration

Matsuno-Gill pattern (Matsuno 1966; Gill 1980)

- Heat-induced tropical circulation composed of Rossby wave and Kelvin wave
- Known to plays crucial roles in Earth's troposphere

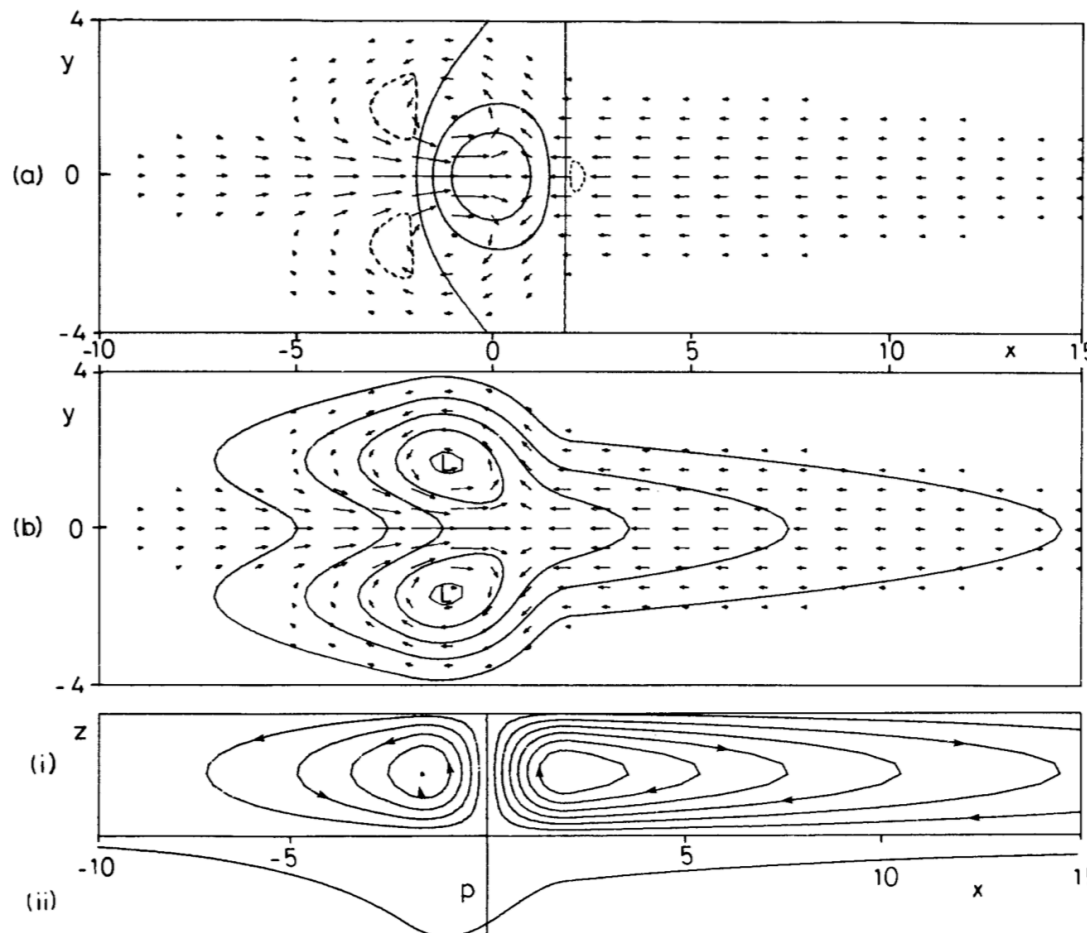


Figure 1. Solution for heating symmetric about the equator in the region $|x| < 2$ for decay factor $\varepsilon = 0.1$.

(a) Contours of vertical velocity w (solid contours are 0, 0.3, 0.6, broken contour is -0.1) superimposed on the velocity field for the lower layer. The field is dominated by the upward motion in the heating region where it has approximately the same shape as the heating function. Elsewhere there is subsidence with the same pattern as the pressure field.

(b) Contours of perturbation pressure p (contour interval 0.3) which is everywhere negative. There is a trough at the equator in the easterly régime to the east of the forcing region. On the other hand, the pressure in the westerlies to the west of the forcing region, though depressed, is high relative to its value off the equator. Two cyclones are found on the north-west and south-west flanks of the forcing region.

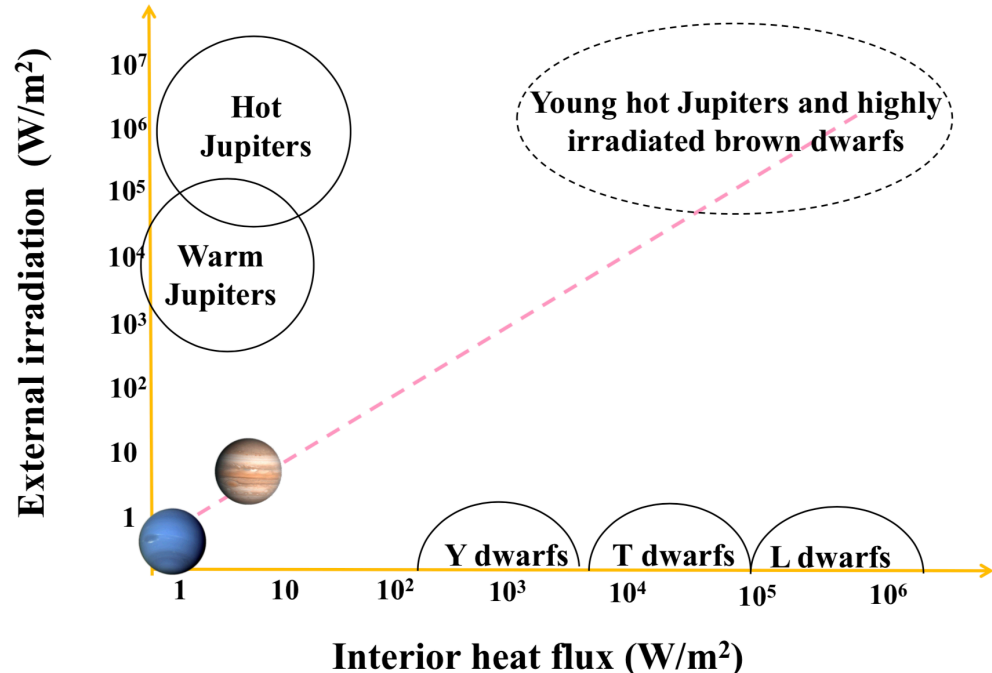
(c) The meridionally integrated flow showing (i) stream function contours, and (ii) perturbation pressure. Note the rising motion in the heating region (where there is a trough) and subsidence elsewhere. The circulation in the right-hand (Walker) cell is five times that in each of the Hadley cells shown in (c).

Horinouchi et al. (2020)との関連？

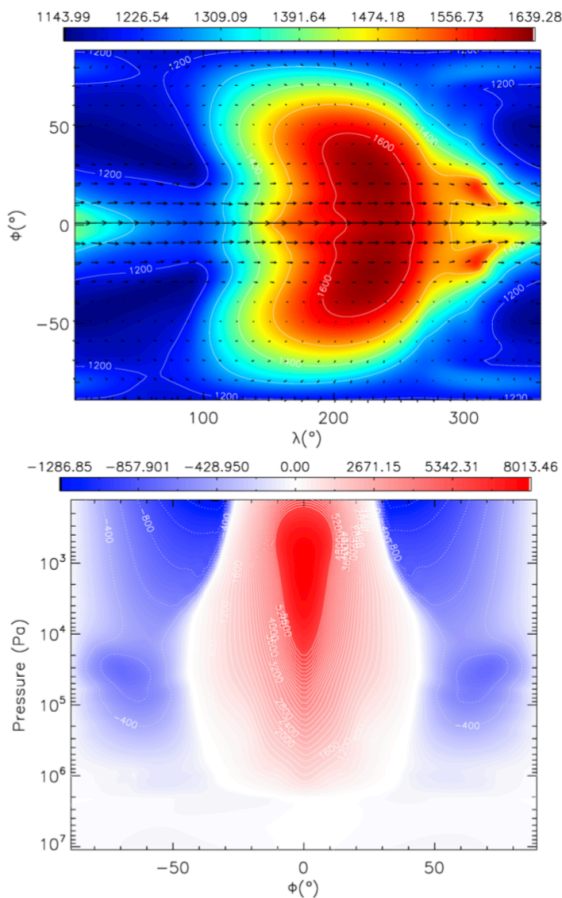
- 金星では、雲追跡によって赤道向き角運動量輸送がとらえられた
→スーパーローテーションに寄与
- 低緯度で日射により励起される熱潮汐波が高緯度まで拡がって減衰することで赤道向き角運動量輸送が起こると解釈
- 热潮汐波の構造は内部位相速度で決まるが、これは大気のスーパーローテーション速度にほぼ等しい
- ホットジュピターでは、日射で励起されるMatsuno-Gillパターンが赤道向き角運動量輸送をもたらすと予想
- 日射加熱パターンは惑星内部（地表）に対して固定しているが、スーパーローテーションの存在下では内部位相速度はスーパーローテーション速度に等しい

両者の共通点、違いはどこに？

Hot Jupitersと太陽系の巨大ガス惑星



Mayne et al. (2017)



Showman et al. (2020)

- これまでのhot Jupiterのモーリングでは外部放射強制での駆動のため比較的浅い循環
- 内部熱源が無視できない場合にはどうなるのか？

まとめ：角運動量輸送機構による分類

Table 2 Classification of the planets according to angular momentum-transporting eddies

Rotation type	Traveling waves generated by instabilities	Solar-locked waves
Slow rotator	Venus	Venus
	Titan	Hot Jupiters
Fast rotator	Jupiter	Tidally-locked terrestrial exoplanets
	Saturn	